Electronic structure, spectra, and properties of 4:2-coordinated materials. I. Crystalline and amorphous SiO_2 and GeO_2†

Sokrates T. Pantelides*
IBM Thomas J. Watson Research Center, Yorktown Heights, New York 10598

Walter A. Harrison
Department of Applied Physics, Stanford University, Stanford, California 94305
(Received 19 March 1975; revised manuscript received 1 October 1975)

A two-parameter tight-binding theory of the electronic structure of 4:2-coordinated materials is proposed. The parameters, a covalent and a polar energy, are fitted to the optical absorption spectra. The valence energy bands and density of states are calculated. In terms of these a consistent interpretation of all the observed photoemission and x-ray-emission spectra of SiO_2 is obtained. The x-ray-absorption spectra are also analyzed. A bond-orbital approximation allows a simple calculation of the refractive index (or dielectric constant) of the various allotropic forms of silica and germania. Finally, the variation in total energy and charge distribution with local distortion is analyzed in order to study structural stability, elastic rigidity, and the effective charges (including dynamic contributions) which determine the piezoelectric constants and infrared absorption intensities.

I. INTRODUCTION

Silicon dioxide (SiO_2) is one of the most common materials in nature. It is the main constituent of more than 95% of all the earth's rocks. Sea sand is essentially pure quartz, one of the various allotropic forms of SiO_2. Most gems, such as amethyst, sapphire, opal, geode, etc, are also quartz containing impurities which impart characteristic colors. Most glasses in our everyday surroundings are made of SiO_2, combined with a variety of other substances. In technology, SiO_2 is present in most devices containing metal-oxide-semiconductor transistors.

For these and other reasons SiO_2 has been studied quite extensively over the years. There exist a variety of measurements of the optical-absorption spectra, both in the uv[1,2] and x-ray region,[3,4] of photoconductivity,[5] x-ray emission spectra (XES),[3,4,6,7] uv and x-ray photoemission spectra (UPS and XPS, respectively),[8,9] and infrared absorption spectra. Much of the theoretical work thus far has attempted to interpret the observed spectra in terms of simple molecular-orbital schemes.[8–11] Quantitative work with rather similar motivations has been carried out by a number of authors using clusters of various sizes.[12–14] Much of the earlier work has recently been reviewed by Ruffa.[15] His conclusion was that the various models were designed to interpret particular spectra, but, in general, when applied to other spectra, they do not do so well. The recent cluster calculations of Yip and Fowler are a step forward,[16] but still, by and large, a comprehensive account of the electronic structure and properties of the various forms of SiO_2 is still lacking.

The purpose of this paper is to present a broad and systematic study of the electronic structure and properties of SiO_2 and GeO_2. The latter has not attracted as much attention as SiO_2 but the two materials can be described in parallel rather conveniently. In a second paper[17] we will turn to other materials of similar coordination but more complicated chemical composition, e.g., $AlPO_4$ (compare with SiO_2 by rewriting it as $SiSiO_4$). The method we will employ is somewhat crude and limited in accuracy but will enable us to address a large number of questions some of which have been unapproachable thus far. More specifically, the method extends the bond-orbital model introduced earlier by Harrison[18] for the study of simple tetrahedral crystals of diamond and zinc-blende structure. The model is based on a linear-combination-of-atomic-orbitals (LCAO) approach which has in the past been used by several authors for various studies.[19,20] The important aspect of the model, which distinguishes it from previous LCAO studies,[11,19,20] is what we have called the *bond-orbital approximation*,[27] which makes the calculation of various properties rather straightforward. The model has thus far been successfully applied to study many properties of simple tetrahedral solids (dielectric constants,[18,21] elastic constants,[22,23] transverse effective charges,[21,24] piezoelectric charges,[21,24] photoelectric thresholds,[21] magnetic susceptibilities,[25] x-ray core shifts,[26] energy bands,[27] etc.). The bond-orbital approximation is also crucial in the present study of 4:2-coordinated materials, for which it naturally takes on a slightly different form.

The plan of this paper is as follows. In Sec. II we describe the crystal structure of the various forms of SiO_2 and GeO_2 and summarize structural

data. In Sec. III we review briefly the bond-orbital model and discuss the bond-orbital approximation as it applies in the present case of SiO_2 and GeO_2. In Secs. IV and V we discuss the valence energy bands and corresponding density of states and interpret the UPS and XPS spectra which probe these levels. In Sec. VI we analyze the optical- and soft-x-ray-absorption spectra. In Sec. VII we make use of the interpretation of the observed spectra to obtain values for the two fundamental parameters of the model. In Sec. VIII we derive an expression for the refractive index and dielectric constant and study its dependence on the structural parameters of the various allotropic forms. In Sec. IX we turn to a study of effective charges, which leads us to address a variety of total-energy-related properties including the determination of the observed Si-O-Si angle, elastic constants, piezoelectricity and infrared absorption intensities. We finish with our conclusions in Sec. X.

II. CRYSTAL STRUCTURES

SiO_2, whose common name is silica, exists in many allotropic forms. Most of them are found in nature in abundant quantities, but some have been made only under laboratory conditions. The best known are quartz, tridymite, cristobalite, and amorphous vitreous silica. Coesite, keatite, stishovite, and melanophlogite are rare forms. With the exception of stishovite, all these forms are built from the same fundamental structural unit, the SiO_4 tetrahedron. In other words, all silicons are surrounded by four oxygens in the tetrahedral directions. At the same time each oxygen is bonded to only two silicons and the Si-O-Si angle, denoted by ϕ, varies from one allotrope to another. This kind of bonding is often referred to as 4:2 coordination. The manner in which the tetrahedra are linked together determines the over-all symmetry, which may be hexagonal, tetragonal, monoclinic, etc. In Table I we list the various forms of silica and the relevant structural information.[28] In Fig. 1 we show a phase diagram for SiO_2 showing at which temperatures and pressures the various forms are stable.[29]

The simplest form of SiO_2 is β-cristobalite (the high-temperature form of cristobalite) which is assumed to have straight Si-O-Si chains with the Si atoms forming a diamond lattice as in the Si crystal. A study of the hexagonal forms of SiO_2 reveals that β-tridymite has its Si atoms in a wurtzite lattice but with the Si-O-Si chains likely to be bent.

GeO_2 is not as polymorphous as SiO_2. It is known to exist in two crystalline forms, a hexagonal quartzlike form and a tetragonal form in which the germaniums are octahedrally coordinated to the oxygens (cassiterite structure) as is stishovite. Finally GeO_2 exists in a vitreous form (vitreous germania) analogous to vitreous silica. The relevant structural parameters are also given in Table I.

III. BOND-ORBITAL APPROXIMATION

For the convenience of the reader and for purposes of introducing notation we first review briefly the bond-orbital approximation as it applies to the simpler tetrahedral solids of diamond and zinc-blende structures.[18,21,27] The starting point of the model is the construction of four tetrahedrally directed sp^3 hybrid orbitals on each atom. This would result in a total of eight orbitals in each primitive unit cell so that an LCAO-type calculation would give rise to an 8×8 secular matrix and to a total of eight bands (four valence bands and the four lowest conduction bands). One can then form bonding combinations of these hybrids, the *bond orbitals*, which for diamond-type crystals are simply given by

$$|b\rangle = [2(1+S)]^{-1/2}(|h_1\rangle + |h_2\rangle) , \tag{1}$$

where h_1 and h_2 are the hybrids on nearest Si atoms pointing toward each other, and S is the overlap

$$S = \langle h_1 | h_2 \rangle . \tag{2}$$

There are four inequivalent bond directions in the crystal and hence four bond orbitals per primitive unit cell. There are, of course, four antibonding orbitals given by

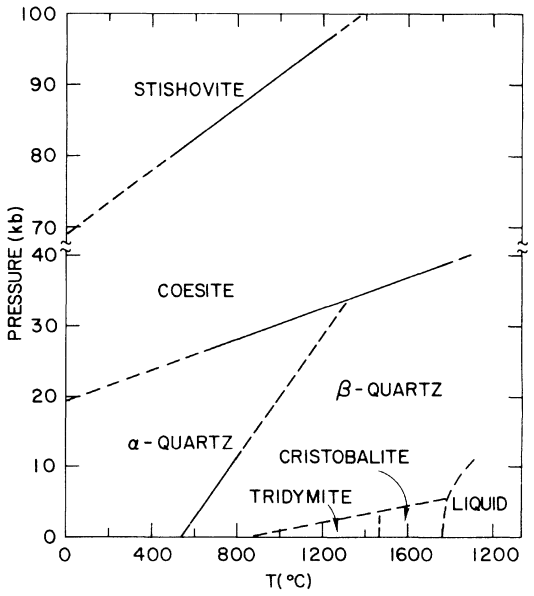

FIG. 1. Phase diagram of SiO_2 (from Ref. 29).

TABLE I. Structural parmeters of the various forms of silica and germania.

Phase	Symmetry	Cell parameters (Å)	Si–O (Å)	O–O (Å)	ϕ (deg)
(A) SiO_2					
α-quartz	Hexagonal	$a=4.913$ $c=5.405$	1.61	2.60–2.67	144
β-quartz	Hexagonal	$a=5.01$ $c=5.47$	1.63	2.60	144 (?)
α-tridymite	Monoclinic (?)	$a=18.54$ $b=4.99$ $c=23.83$ $\beta=105.6°$	?	?	?
β-tridymite	Hexagonal	$a=5.03$ $c=8.22$	1.52	2.57	?
α-cristobalite	Tetragonal	$a=4.973$ $c=6.926$	1.59	2.58–2.63	147
β-cristobalite	Cubic	$a=7.16$	1.55	2.53	180
Keatite	Tetragonal	$a=7.456$ $c=8.604$	1.57–1.61	?	?
Coesite	Monoclinic (hexagonal)	$a=7.17$ $b=12.38$ $c=7.17$ $\beta=120°$	1.60–1.63	2.60–2.67	120
Stishovite[a]	Tetragonal	$a=4.179$	?	?	?
Melanophlogite	Cubic	$a=13.402$	?	?	?
Fibrous silica	Orthorhombic	$a=8.36$ $b=5.16$ $c=4.75$	?	?	?
Vitreous silica	Amorphous	•••	1.61	2.63	$\langle 144 \rangle$[b]
(B) GeO_2					
Germania quartz	Hexagonal	$a=4.972$ $c=5.648$	1.74	2.84	130
Tetragonal germania[a]	Tetragonal	$a=4.395$ $c=2.859$	1.86	?	$\langle 90 \rangle$[b]
Vitreous germania	Amorphous	•••	?	?	?

[a]These forms have the rutile structure so that each silicon (or germanium) is surrounded by six oxygens in the octahedral directions.

[b]The brackets $\langle\ \rangle$ indicate averages.

$$|a\rangle = [2(1-S)]^{-1/2}(|h_1\rangle - |h_2\rangle)\ , \qquad (3)$$

for a total of eight orbitals. The corresponding 8×8 matrix differs from the 8×8 matrix of the hybrids by a unitary transformation and thus would result in the same eight bands as before. This unitary transformation of the eight hybrids into four bonding and four antibonding orbitals is very crucial, however, because the $|a\rangle$ and $|b\rangle$ at the same site do not interact. One can then assume that off-diagonal coupling between $|a\rangle$'s and $|b\rangle$'s at different sites is small, and concentrate on the four valence bands arising completely from the four bond orbitals. As a consequence, one can obtain the total electronic energy by simply evaluating the trace of the 4×4 matrix. Since this trace turns out to be independent of k *one does not have to solve the band problem in order to calculate total energies*. In other words, the total electronic energy is simply proportional to the sum of

bond energies and the total charge density is proportional to the charge density of the bond orbitals. Since most response functions are measures of distortions imposed on the total energy, and one is able to calculate the total energy in the presence of external perturbations, one can explicitly and simply calculate dielectric constants, elastic constants, effective charges (caused by redistribution of the charge density), etc.

The importance of the bond-orbital approximation is immediately and explicitly seen when we turn to the bond orbitals of zinc-blende-type compounds. Because the two atoms participating in a bond are no longer identical, the bond orbital is not the simple form (1). One must write

$$|b\rangle = u_a|h_a\rangle + u_c|h_c\rangle \ , \tag{4}$$

where a stands for anion, the nonmetallic ion, and c for cation, the metallic ion, and u_a and u_c are numerical coefficients. Now, because of the bond-orbital approximation, the total electronic energy per unit volume is given by $8N\langle b|H|b\rangle = 8N\epsilon_b$, where N is the density of valence electrons and H is the crystal Hamiltonian. Thus, minimizing ϵ_b is equivalent to minimizing the total electronic energy. The result is simple when the overlap S is neglected.[30] It may conveniently be expressed

$$|b\rangle = [\tfrac{1}{2}(1+\alpha_p)]^{1/2}|h_a\rangle + [\tfrac{1}{2}(1-\alpha_p)]^{1/2}|h_c\rangle \ , \tag{5}$$

where α_p, which is a measure of how polar the bond is, and is therefore called the *polarity*, is given by[31]

$$\alpha_p = V_3/(V_2^2+V_3^2)^{1/2} \ . \tag{6}$$

A more complicated expression is obtained for $|b\rangle$ when S is included.[30] The expression for α_p remains unchanged, however. V_2 and V_3 are the following matrix elements:

$$V_2 = -\langle h_a|H|h_c\rangle/(1-S^2) \ , \tag{7}$$

$$2V_3 = (\langle h_c|H|h_c\rangle - \langle h_a|H|h_a\rangle)/(1-S^2)^{1/2} = (\epsilon_c - \epsilon_a)/(1-S^2)^{1/2} \ . \tag{8}$$

The bond energy ϵ_b is given by

$$\epsilon_b = \tfrac{1}{2}(\epsilon_a+\epsilon_c) + SV_2 - (V_2^2+V_3^2)^{1/2} \ . \tag{9}$$

For a homopolar diamond-type crystal $V_3 = 0$, $\alpha_p = 0$.

We now turn to an analogous bond-orbital description of SiO_2. For purposes of motivation we start with the ideal β-cristobalite structure which is presumed to be a diamond lattice of Si atoms with O atoms inserted at each bond site. The natural choice of orbitals is then sp^3 hybrids on the Si's, as in the Si crystal, plus the three oxygen $2p$ states (the oxygen $2s$ states are essentially core states; we will have occasion to discuss this later on). Thus associated with each bond site we now have a total of five orbitals, $\{h_1, h_2, p_x, p_y, p_z\}$, or, equivalently, $\{b, a, p_x, p_y, p_z\}$, where b and a are as in (1) and (3). Either set would give us a 20×20 matrix and 20 bands (because of the four inequivalent bond sites), only 12 of which would be occupied. The other eight would be the lowest conduction bands. We thus seek three linear combinations of the five orbitals which will be orthogonal to the remaining two, whereby a bond-orbital approximation that decouples the occupied from the empty bands will become possible. This step is analogous to forming the bonds $|b\rangle$ [Eq. (1)] in the diamond-type crystals and seeking the linear combinations (4) in the zinc-blende-type compounds. In the case of β-cristobalite, the task is still rather simple because from among the five orbitals $\{b, a, p_x, p_y, p_z\}$ only $|a\rangle$ and $|p_z\rangle$ interact. [For choice of axes see Fig. 2(a).] We thus form some kind of superbond orbital which we write

$$|B\rangle = u_z|p_z\rangle + u_a|a\rangle \ . \tag{10}$$

There exists, of course, a corresponding antibonding combination $|A\rangle$ so that $\langle B|A\rangle = 0$. We thus have a set of five noninteracting orbitals, namely $\{B, A, b, p_x, p_y\}$. At this stage we impose the bond-orbital approximation and neglect off-diagonal elements between the subset $\{B, p_x, p_y\}$, which gives rise to the 12 full valence bands, and the subset $\{b, A\}$ which gives rise to the lowest conduction bands. The approximation is particularly good in this case in view of the relatively large gap between valence and conduction bands,

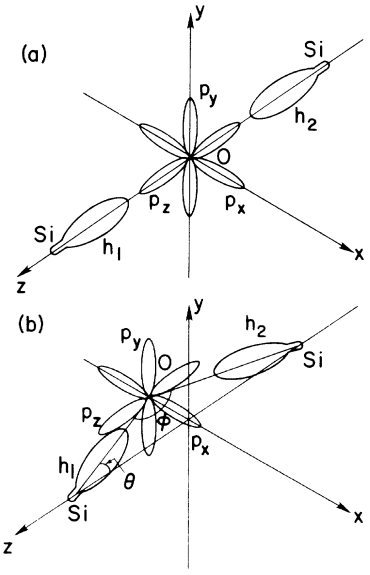

FIG. 2. Orbitals and choice of axes in the case of (a) β-cristobalite; (b) the other forms of SiO_2.

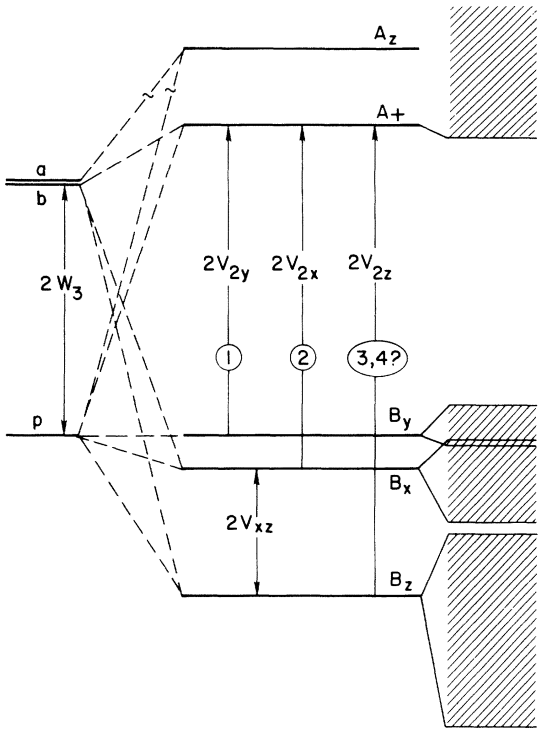

FIG. 3. Schematic of the occupied and empty orbitals in SiO_2 from which the valence and conduction bands are formed.

9 eV.[5] As a consequence, the trace of the 12×12 matrix arising from $\{B, p_x, p_y\}$ gives us once more the total electronic energy whereby we can minimize $\langle B|H|B\rangle$ with respect to u_z and u_a of Eq. (10). The result is analogous to (5) (when $S=\langle a|p_z\rangle$ is neglected), but, instead of α_P, for the corresponding polarity we employ the notation[32] β_p:

$$|B\rangle=[\tfrac{1}{2}(1+\beta_p)]^{1/2}|p_z\rangle+[\tfrac{1}{2}(1-\beta_p)]^{1/2}|a\rangle\ . \quad (11)$$

The definition of β_p is similar to (6), but slightly different:

$$\beta_p=w_3/(2W_2^2+W_3^2)^{1/2}\ , \quad (12)$$

where we use W's instead of V's for "internal"[32] interactions. The W's are defined by

$$W_2=-\langle h|H|p_z\rangle/(1-2S^2)\ , \quad (13)$$

$$2W_3=(\langle a|H|a\rangle-\langle p_z|H|p_z\rangle)/(1-2S^2)^{1/2}$$
$$=(\epsilon_a-\epsilon_z)/(1-2S^2)^{1/2}\ , \quad (14)$$

where

$$S=\langle h|p_z\rangle\ . \quad (15)$$

The extension to treat the more general SiO_2 crystal, or vitreous silica, in which the Si-O-Si chains are not straight ($\phi\neq180°$), is straightforward. The Si hybrids are still constructed to point in the direction of the oxygens (tetrahedral directions) and the set is once more extended to include $|p_x\rangle$, $|p_y\rangle$, and $|p_z\rangle$ orbitals on the oxygens [Fig. 2(b)]. We again form $|b\rangle$ and $|a\rangle$ as before and the basis set becomes $\{b, a, p_x, p_y, p_z\}$. When we allow these orbitals to interact, the new symmetry allows mixing between $|p_z\rangle$ and $|a\rangle$, as before, and also between $|p_x\rangle$ and $|b\rangle$. We thus form two new superbond orbitals: $|B_z\rangle$, as in (10), and an analogous $|B_x\rangle$. The occupied orbitals are now $\{B_z, B_x, B_y\}$, (where for uniformity we defined $|B_y\rangle=|p_y\rangle$) and the empty ones are the corresponding $\{A_z, A_x\}$. These levels are illustrated in Fig. 3. Other designations in that figure will be discussed later. The same minimization-of-total-electronic-energy procedure yields

$$|B_z\rangle=[\tfrac{1}{2}(1+\beta_{p_z})]^{1/2}|p_z\rangle+[\tfrac{1}{2}(1-\beta_{p_z})]^{1/2}|a\rangle\ , \quad (16)$$

$$|B_x\rangle=[\tfrac{1}{2}(1+\beta_{p_x})]^{1/2}|p_x\rangle+[\tfrac{1}{2}(1-\beta_{p_x})]^{1/2}|b\rangle\ , \quad (17)$$

where

$$\beta_{p_z}=W_{3z}/(2W_{2z}^2+W_{3z}^2)^{1/2}\ , \quad (18)$$

$$\beta_{p_x}=W_{3x}/(2W_{2x}^2+W_{3x}^2)^{1/2}\ . \quad (19)$$

It might look that the problem is getting excessively complicated, but, in actuality, the entire description is based on just two matrix elements, W_2 and W_3 as defined in (13) and (14). A rather straightforward calculation results in

$$W_{2z}=W_2\left(\frac{1-2S^2}{1-2S^2\cos^2\theta}\right)\cos\theta\ , \quad (20a)$$

$$W_{2x}=W_2\left(\frac{1-2S^2}{1-2S^2\sin^2\theta}\right)\sin\theta\ . \quad (20b)$$

[See Fig. 2(b) for the definition of θ. It is given by $\theta=\frac{1}{2}(180-\phi)$.] W_{3x} and W_{3z} are given by expressions analogous to (14), but, to a good approximation, one can take $W_{3x}=W_{3z}=W_3$. It is clear that all the quantities of interest are simple analytical functions of W_2, W_3, and the angle θ. We will extract values for W_2 and W_3 from experimental data in Sec. VII. We may just note one more thing here, namely that the bond energies are given by

$$\epsilon_{B_z}=\langle B_z|H|B_z\rangle=\sqrt{2}S_zW_{2z}-(2W_{2z}^2+W_3^2)^{1/2}\ , \quad (21)$$

$$\epsilon_{B_x}=\langle B_x|H|B_x\rangle=\sqrt{2}S_xW_{2x}-(2W_{2x}^2+W_3^2)^{1/2}\ , \quad (22)$$

where $S_z=S\cos\theta$ and $S_x=S\sin\theta$.

IV. ENERGY BANDS AND DENSITY OF STATES

As we noted already, within the bond-orbital approximation, the problem of the energy bands is separate from the calculation of other properties which depend only on the trace of the secular matrix. The energy bands are essentially determined by the off-diagonal matrix elements, namely

the interactions between bond orbitals at *different* bond sites. The band structure is of course interesting because it can be used to interpret photoemission spectra, x-ray-emission spectra and optical-absorption spectra. However, a valuable feature of the bond-orbital approximation is that one does not need the bands at all in order to calculate other properties.

We turn first to the valence bands, which are determined by the minimal basis set $\{B_x, B_y, B_z\}$ (recall that $B_y = p_y$ and, in the case of β-cristobalite $B_x = p_x$) at each bond site, which for SiO_2 and GeO_2 means at each oxygen site. The size of the secular matrix depends on how many bond sites there are in the primitive unit cell. For β-cristobalite (diamond-lattice, full O_h^7 symmetry) there are four bond sites (oxygens) per primitive cell (i.e., there are four distinct bond directions in the diamond lattice) which results in a 12×12 secular matrix and 12 bands, just enough to accomodate the 24 electrons per primitive unit cell. In quartz, on the other hand, there are six oxygens per primitive unit cell for a total of 18 valence bands. In each case one could in principle get the bands to any accuracy by including an adequate number of distant-neighbor interactions.

The simplest case is of course β-cristobalite. The calculation of the valence bands[33] has a number of similarities with the corresponding calculation for Si (Ref. 27). Both crystals have the full symmetry of the diamond lattice (O_h^7). In the case of Si, we had one bond orbital b at each bond site which gave us a 4×4 matrix. The bands were adequately described by retaining only two matrix elements, B_1 between adjacent bonds and B_4 between second-neighbor bonds along the same direction. In the present case of β-cristobalite we have three bond orbitals, p_x, p_y, and B_z, at each bond site. The result will of course be a 12×12 matrix, but we may expect that each of the three bond orbitals will give rise to a 4×4 submatrix along the diagonal which is analogous to the 4×4 matrix of Si. It turns out that B_z does indeed give such a 4×4 submatrix, but p_x and p_y cannot be split up. The reason is that, by symmetry, the x and y axes cannot be uniquely defined. The resulting 8×8 submatrix comes purely from oxygen p orbitals, whereby the nearest-neighbor interactions can be expressed entirely in terms of two matrix elements, as has been shown in the case of the p bands of rocksalt-type compounds[34]: V_p for p orbitals pointing toward each other, and V_π for p orbitals pointing in directions perpendicular to the vector connecting the two atoms. In Ref. 34 V_π was found to be a 12% correction to V_p and therefore we drop it completely in this study.

For the final calculation of the valence bands of cristobalite we retained V_p for interactions between the p orbitals and B_1 for interactions between the B_z orbitals. B_1 is in turn expressible in terms of V_p and V_1, the matrix element between two Si hybrids on the same atom, as defined and evaluated in Ref. 27. Assuming the bond energies ϵ_x, ϵ_y, and ϵ_{B_z} along the diagonal are known (Sec. VIII), only a value for V_p is needed before the bands may be calculated. The value used here is $V_p = 1.45$ eV, estimated from the observed total width. (See Sec. VII.) The resulting bands and density of states are given in Fig. 4. The symmetry designations for the bands uses the notation of Ref. 35 and have been determined by standard group-theoretic arguments.

The bands are rather interesting in themselves but we shall postpone a detailed study of them to another paper.[36] The interesting observation for our present purposes is that the "nonbonding" p bands are rather wide and give rise to peaks, which, when viewed from a Si atom, have either odd (mostly p like) character (high-energy peaks) or even (s like) character (low-energy peak). The "bonding" bands follow at even lower energies. Note that though these bands are not quite like the Si valence bands, due to strong interactions with the nonbonding bands, they nevertheless give rise to a p-like peak, a mixed s-p peak and a predominantly s-like peak. The gap between bonding and nonbonding bands is produced by the strong interactions between the two sets of bands. If these interactions were turned off (so that the 12×12 matrix separates into an 8×8 and a 4×4 submatrices), the two sets of bands overlap considerably.[36]

We have not attempted to calculate the valence bands of any other form of SiO_2 at this time. We expect the bands will look very different in the other forms (e.g., as we saw, quartz actually has 18 valence bands and a hexagonal Brillouin zone). On the other hand the density of states will probably not vary appreciably. This is born

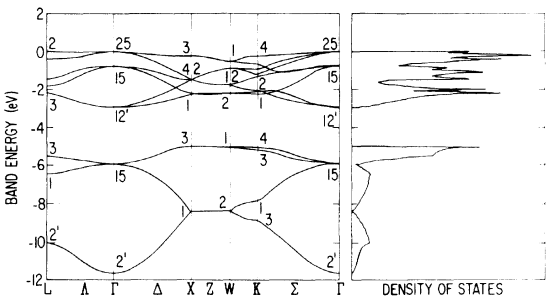

FIG. 4. Valence bands and density of states of β-cristobalite.

out, for example, from the study of Joannopoulos and Cohen[37] who calculated bands and densities of states for Si in various hypothetical crystal structures. We do expect one important change, however. For bent Si-O-Si chains the x and y axes (Fig. 2) are no longer equivalent so that $\epsilon_x \neq \epsilon_y$. The eight nonbonding bands would then split into four p_y bands which are truly nonbonding (except for some hybridization) and four B_x bands which are also bonding, though not as much as the B_z bands. We have attempted to simulate this effect by evaluating the β-cristobalite bands with ϵ_x lying 1.5 eV below ϵ_y (see Sec. VII for this choice). The value of ϵ_z was also changed to that appropriate for bent chains (see Sec. VII). The resulting bands and density of states are shown in Fig. 5. As one might expect, the x-y bands show more peaks in the density of states. The net result is a predominantly s-like and a predominantly p-like peak from each subset of bands.

Finally, we can attempt to simulate the density of states of *amorphous* vitreous silica by referring to the well-known results, both theoretical[37] and experimental,[38] on amorphous Si. This is shown in Fig. 5 by the dashed line in the density of states; it amounts to a filling up of the dip between the two lower-energy peaks. Recent unpublished experimental data[39] on amorphous and crystalline SiO_2 show that this is in fact the only difference in the two spectra.

V. INTERPRETATION OF PHOTOEMISSION AND X-RAY-EMISSION SPECTRA

No experimental data are available on β-cristobalite. (The existence of a form with straight Si-O-Si chains has not actually been conclusively established.) It is therefore not possible to provide a direct experimental verification of the explicit calculations of Sec. IV. The analysis we presented, however, enables us to provide a systematic interpretation of all the observed photoemission and x-ray-emission spectra on other polymorphs.

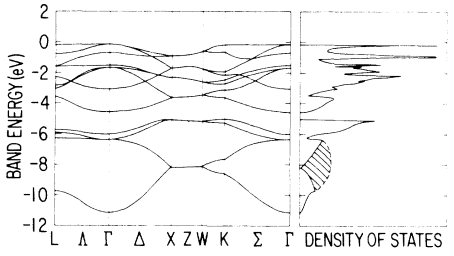

FIG. 5. Valence bands and density of states for a hypothetical system with the atomic positions of β-cristobalite but with $\epsilon_x \neq \epsilon_y$. See text.

In photoemission one illuminates the sample with light of given energy and measures the kinetic energy of the emitted electrons. The resulting spectrum is assumed to resemble the density of occupied states except possibly for the heights of peaks, which may change by matrix-element effects. In particular, uv photoemission (UPS) picks out p electrons more strongly than s electrons whereas x-ray photoemission (XPS) does the opposite.

In x-ray emission one first bombards the sample with high-energy electrons which create holes in the inner shells of the atoms. Valence electrons then drop into these empty states by emitting x rays. Again the observed spectrum resembles the valence density of states, but matrix-element effects are now more pronounced. For example, when the core level is an s state the corresponding s-like valence levels are suppressed almost totally. The various x-ray-emission spectra are usually identified by the spectroscopic notation of the relevant core level.

For SiO_2 there exist both UPS and XPS data, taken on amorphous samples. We show these in Fig. 6 along with the x-ray-emission spectra of Si $1s$ (Si $K\beta$), Si $2p$ (Si $L_{2,3}$) and O $1s$ (O $K\alpha$) core levels taken on crystalline quartz samples. In all the spectra in Fig. 6 we do not show the O $2s$ peak, which occurs at about -21 eV. By making use of the theoretical description of the valence bands given in Sec. IV these spectra could be positioned on the energy axis as shown leading to a consistent interpretation for all of them. In all cases the zero of energy marks the top of the valence bands. The numbers in parentheses under the labels of the XES spectra denote the position (in eV) of the corresponding core level from the valence-band top.

The basic premise used was that the nonbonding bands arising from B_x and B_y each give rise to a predominantly s-like and a predominantly p-like peak and that XPS emphasizes s peaks while UPS emphasizes p peaks. In addition, the selection rules for the XES spectra, namely that s core levels pick out the p peaks and p core levels pick out the s peaks, were used. The consistent interpretation arrived at is illustrated in Fig. 6 by the vertical lines through the panels. It should be noted that the top panel, marked "theory," was only used as a guide as to what kind of structure one might expect. It should not be viewed as a direct prediction of the experimental spectra.

The correctness of the positioning of the XES spectra in Fig. 6 can be verified directly by measuring the position of the core levels relative to the top of the valence bands by XPS. These have recently been measured[39] and are in excellent agreement with the values shown in Fig. 6.

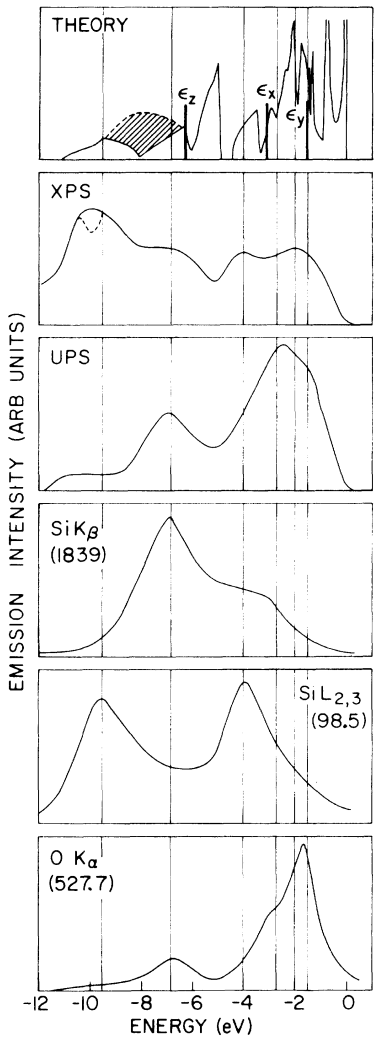

FIG. 6. Photoemission (XPS and UPS) and x-ray emission spectra of SiO_2 positioned on the energy axis so that the zero of energy marks the top of the valence bands. The top panel is a simulation of the density of states of the valence bands as described in the text.

A few words about each spectrum are in order. Starting with the bottom panel of Fig. 6, the O $K\alpha$ spectrum, we note that the main peak arises from the nonbonding oxygen p_y orbitals while the shoulder on the left arises from the "partially-bonding" oxygen p_x orbitals. The height of this feature is reduced because p_x is a component of B_x and its population is reduced by the factor $[\frac{1}{2}(1+\beta_{p_x})]^{1/2}$ appearing in Eq. (17). Since $\beta_{p_x} = 0.73$ (Sec. VII), this would predict a reduction in intensity of about 15% which is in good agreement with experiment.[40] The lower peak farther on the left arises from the p_z oxygen orbitals which are components of B_z [Eq. (16)]. The reduction in intensity is now determined by the factor $[\frac{1}{2}(1+\beta_{p_z})]^{1/2}$ which comes out to be 65%, again in rather good agreement with experiment. The overall interpretation of this spectrum is in good agreement with interpretations proposed previously.[11,13,14,41]

The Si $L_{2,3}$ spectrum consists of two main peaks[42,43] which, from atomic symmetry considerations, sample Si s-like states in the valence bands. The B_y bands have no such components and thus do not appear in this spectrum. The two observed peaks thus arise from the B_x and B_z bands. Notice, however, that the peak on the right *does not* coincide with the corresponding peak in the O $K\alpha$ spectrum. This demonstrates the importance of *banding* in the B_x orbitals as noted earlier: owing to band-structure effects, the B_x orbitals give rise to an s-like peak, picked out by Si $L_{2,3}$, and a p-like peak, picked out by O $K\alpha$. Thus the orbital energy of B_x cannot in principle account for all the observed spectra, which explains the failure of previous attempts to interpret all the spectra in in terms of molecular orbitals. This is the first time that *band-structure effects* are shown to be important in obtaining a consistent interpretation of all the observed spectra. Similarly, the peak on the left corresponds to the s-like peak of the B_z bands. Again, the importance of band-structure effects is demonstrated. The relative heights of these two peaks, however, are not directly interpretable (one would expect the low-energy peak to be stronger).

The Si $K\beta$ spectrum is expected to sample the Si p-like states in the valence bands. Once more, the B_y bands do not appear. A strong peak arises from the B_z bands which corresponds to the same peak picked out by the O $K\alpha$ spectrum. A smaller feature on the right corresponds to the p peak of the B_x bands as in the O $K\alpha$ spectrum. Note that the intensity ratios are now essentially reversed because the Si orbitals are more heavily occupied in B_z states rather than the B_x states [Eqs. (16) and (17)] while the opposite was true for the oxygen orbitals.

Finally, it is clear that the UPS and XPS spectra sample all the peaks mentioned above, but with different emphasis. Note, however, that these spectra were taken on amorphous samples. The dotted line in the leftmost peak of the XPS spectrum (Fig. 6) is drawn to indicate what the spectrum might look like for a crystalline sample.

Figure 6 also helps illustrate another important point, namely that trying to extract total bandwidths and/or band edges from XES spectra may be an unreliable procedure because some structure near the edge may be totally wiped out by vanishing matrix elements. This difficulty is particularly evident in the Si $L_{2,3}$ and Si $K\beta$ panels of Fig. 6 where the band edge is seen to be considerably higher than any extrapolation of the tail would

indicate. XPS spectra seem to be the best choice for extracting bandwidths and edges.

VI. OPTICAL- AND SOFT-X-RAY-ABSORPTION SPECTRA

We turn now to the excited states of these crystals. At this stage, in the absence of a full band calculation, only qualitative arguments can be made. The tight-binding scheme of Sec. IV is not suitable for calculating conduction bands but it can give an indication as to what orbitals will give rise to them and at what energies the oscillator strength with the valence bands is concentrated. For example, in Si the valence bands arise from the bond orbitals $|b\rangle$ [Eq. (1)] while the conduction bands arise from the corresponding antibonding orbitals $|a\rangle$ [Eq. (3)]. Similarly, we can expect the conduction bands in SiO_2 to arise from the antibonding orbitals $|A_x\rangle$ and $|A_z\rangle$. (There is no $|A_y\rangle$ because $|B_y\rangle = |p_y\rangle$.) Other orbitals that may be present are the O $3s$ orbitals and the Si $3d$ orbitals though the latter are safely neglected[42] in view of the fact that in Si the $3d$ bands lie rather high in energy. The position of $|A_z\rangle$ may be inferred in a straightforward manner (Sec. VII) to lie high in energy. $|A_x\rangle$, however, interacts with the O $3s$ orbital giving two states $|A_+\rangle$ and $|A_-\rangle$ ("bonding" and "antibonding" combinations). $|A_-\rangle$ is likely to be pushed at high energies leaving $|A_+\rangle$ to give rise to the lowest conduction bands. Its composition is

$$|A_+\rangle = c_1|b\rangle + c_2|p_x\rangle + c_3|3s\rangle\,, \tag{23}$$

where the coefficients cannot be determined explicitly. In β-cristobalite, however, with $\phi = 180°$, $c_2 = 0$. The symmetry of $|A_+\rangle$ is then even, much like $|b\rangle$, and, in β-cristobalite, it will give rise to four bands, resembling the *valence* bands of Si. The resulting symmetries at Γ will be Γ_1 (fully symmetric) and $\Gamma_{25'}$.

A. Optical-absorption spectra

The first spectrum of interest arises from excitations of the valence electrons to the conduction-band states and to excitons constructed therefrom. This can be measured by optical absorption,[1,2] by energy-loss experiments[9,44] or photoyield experiments. It is also the hardest to interpret because of dispersion in both in the initial and final bands and because of excitonic effects. The presence or absence of the latter can be checked to a certain extent by measuring the band gap with an independent experiment, such as photoconductivity.

The optical-absorption spectrum[1] of SiO_2 is shown in the top panel of Fig. 7 by the solid line. The dashed line is the energy-loss spectrum for the same excitations as measured recently by Koma and Ludeke.[44] The vertical line at 9 eV

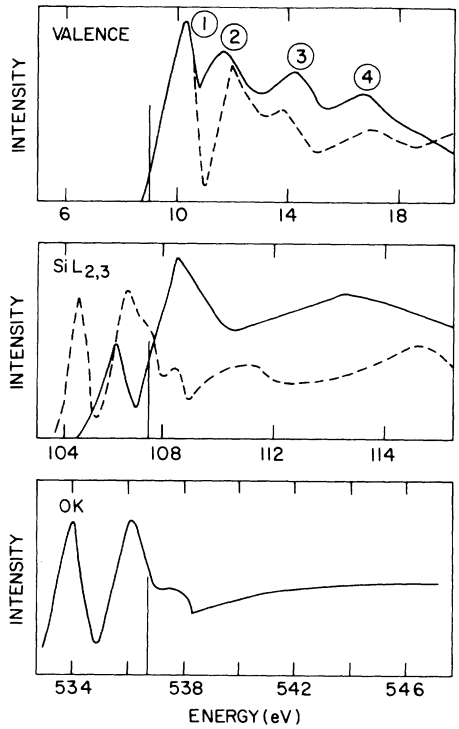

FIG. 7. Valence- and core-electron excitation spectra of SiO_2. Top panel: solid line from Ref. 1, dashed line from Ref. 44; middle panel: solid line from Refs. 3 and 4, dashed line from Ref. 44; bottom panel: from the conduction-band edge.

marks the band gap as measured by photoconductivity by DiStefano and Eastman.[5] The absence of structure below 9 eV signifies that excitons are absent in this material. This is analogous to the tetrahedral semiconductors where excitons have small binding energies and little oscillator strength requiring high-resolution data to resolve. In fact it may suggest that the band gap is indirect.

This analogy with tetrahedral semiconductors suggests that the observed spectrum may be interpreted by analogies with the optical spectrum of Si. In that case the excitations are from the bonding $|b\rangle$ bands to the antibonding $|a\rangle$ bands and the result is one prominent peak, usually denoted by E_2. This was actually identified by Harrison and Ciraci[21] to represent the bonding-antibonding separation denoted[21] by $2V_2$. We may therefore expect similar peaks arising from excitations from the bond orbitals $|B_x\rangle$, $|B_y\rangle$, and $|B_z\rangle$ to the antibonding orbitals $|A_+\rangle$ and $|A_z\rangle$. Symmetry, however, forbids some of these excitations. In Fig. 8 we show a pictorial of all the orbitals indicating by arrows those of the transitions that are allowed. The numbers in the circles represent

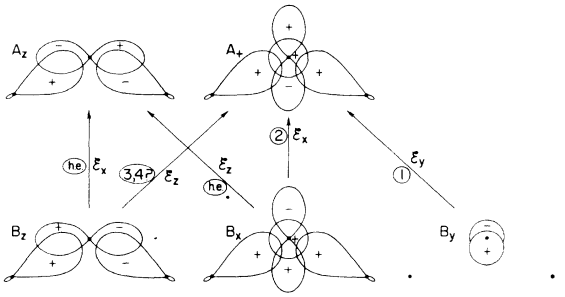

FIG. 8. Pictorial representation of the bonding orbitals B_x, B_y, B_z and the antibonding orbitals A_z and A_+. The arrows denote the allowed transitions. The labels are the component of the electric field $\mathcal{E}$ that makes the transition possible and the number of the peak (compare Fig. 6, top panel) with which the transition is tentatively identified.

tentative identification of the transition with the peaks in Fig. 7, top panel. "h. e." denotes high-energy excitations. We may note that our interpretation is similar to that of Ibach and Rowe[9] in that we identify a single excited state being responsible for the observed spectrum. Our assignment of initial states is, however, different.

If our assignments for the first two peaks in the SiO_2 spectrum are correct, we are able to predict the corresponding peaks in GeO_2 (see Sec. VII). The first peak is predicted to lie at 11.1 eV. The experimental spectrum[45] is shown in Fig. 9. The structure around 6–7 eV is probably not due to excitations in bulk GeO_2. (Phillips[46] has suggested it is due to a metastable GeO_x layer on the surface.) This structure is then followed by a distinct peak at 11.0 eV, which compares very well with our prediction of 11.1 eV (Fig. 9). Above the first peak at 11 eV, however, GeO_2 does not show the distinct peaks observed in SiO_2. We nevertheless indicate our predictions for the locations of these peaks. We observe that these peaks are now more closely spaced which may be responsible for the rather washed out structure.

B. Soft-x-ray-absorption spectra

The x-ray-absorption spectra (or x-ray energy-loss spectra) might be expected to give more direct information about the excited states of crystal because the initial states (core levels) are dispersionless. This would in fact be true if excitonic effects were not present whereby the final states would be the conduction-band states. The presence or absence of excitons can again be checked by an independent determination of the conduction-band edge relative to the core level. This can be done by a simple addition of the energy separation between the core level and the top of the valence band from XPS or XES spectra and the valence-to-conduction-band gap. The validity of this approach is a rigorous theorem proved recently by one of us (S.T.P.).[47,48]

In Fig. 7, in the lower two panels, we show the Si $L_{2,3}$ and O K excitation spectra from Refs. 3, 4, and 41. The conduction-band edge in each panel is denoted by the solid vertical line. The three panels are positioned with respect to each other so that the three band edges coincide, in order to facilitate discussion. This makes clear that the interpretation given by Koma and Ludeke[44] for the three spectra cannot be supported.

The most interesting feature of the two core spectra in Fig. 7 is the presence of structure below the band edge which signifies the presence of excitons. This is in agreement with the analysis of the respective spectra in insulators[47] where excitons were found to be dominant with large binding energies and also the tetrahedral crystals where excitons are also present.[49–51] Koma and Ludeke[44] appear to have resolved the core exciton in the $L_{2,3}$ spectrum of Si and have also seen a surface state below it.

The interpretation of the two core spectra in Fig. 6 cannot be conclusive at this time. Both of them exhibit a prominent peak at about 2.5 eV below the band edge (the band edge is of course uncertain by about 0.5 eV). Alkali halides have been shown[47] to have core excitons with binding energies of several eV, whereby an interpretation of the observed peaks in the SiO_2 soft-x-ray spectra may very well be excitons with binding energies of about 2.5 eV. The possibility of surface states (both true surface states or states associated with internal dangling bonds present in the amorphous phase) cannot be ruled out, however.

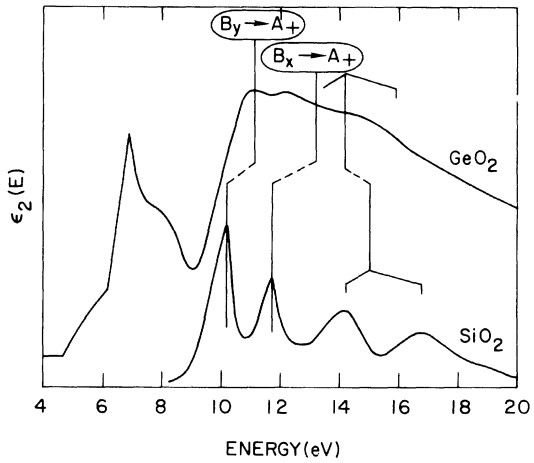

FIG. 9. Optical-absorption spectrum of GeO_2 compared with that of SiO_2.

TABLE II. The parameters of the model for SiO_2 (quartz) and quartzlike GeO_2. Note that only W_2 and W_3 are the two fundamental parameters determined from experimental data on SiO_2. All other quantities, including all GeO_2 parameters (other than d and ϕ) are derived from these.

Parameter	SiO_2 (quartz)	GeO_2 (quartzlike)
d	1.61 Å	1.74 Å
ϕ	144°	130°
θ	18°	25°
S	0.3	0.3
S_x	0.093	0.127
S_z	0.285	0.272
W_3	4.35 eV	4.49 eV
W_2	10.75 eV	9.13 eV
W_{2x}	2.77 eV	3.30 eV
W_{2z}	10.00 eV	7.96 eV
V_{2x}	5.85 eV	6.60 eV
V_{2y}	5.10 eV	5.55 eV
V_{2z}	7.48 eV	7.26 eV
V_{xz}	3.26 eV	1.32 eV
β_{px}	0.73	0.68
β_{py}	1.00	1.00
β_{pz}	0.29	0.37
Z^* on O	−1.02 $\lvert e \rvert$	−1.05 $\lvert e \rvert$

VII. DETERMINATION OF FUNDAMENTAL PARAMETERS

Before we proceed to study further properties it is useful to obtain values for the fundamental parameters of our model, which are basically two, W_2 and W_3. The description of the valence and excited states given thus far enables us to do that in a convenient way.

For this purpose we refer to Fig. 3. The diagram contains in a concise and illustrative fashion all our assignments. We denoted the excitation energies by $2V_{2x}$, $2V_{2y}$, and $2V_{2z}$ in analogy with

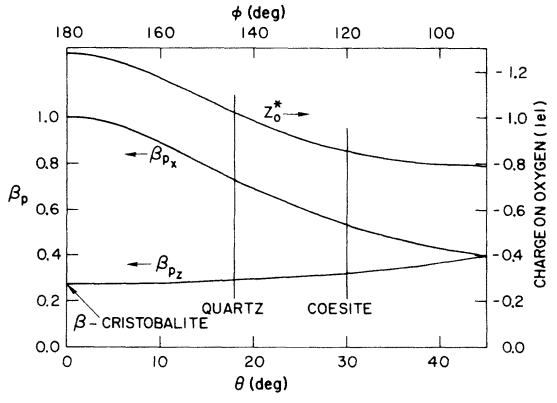

FIG. 10. Polarities β_{px} and β_{pz} of SiO_2 as functions of the Si-O-Si angle. Also shown is the net effective charge on the oxygens.

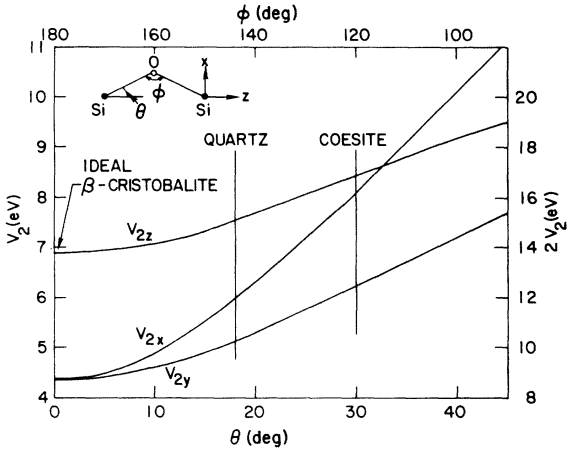

FIG. 11. Quantities V_{2y} and V_{2x} (corresponding to the first two optical-absorption peaks at $2V_{2y}$ and $2V_{2x}$) and V_{2z} as functions of the Si–O–Si angle.

the notation $2V_2$ employed for Si in Ref. 21. This will be useful in Paper II (Ref. 18) where the present picture is extended to study $AlPO_4$ and other compounds. In terms of the W's introduced in Sec. III it is rather straightforward to obtain

$$2V_{2x} = 2(2W_{2x}^2 + W_3^2)^{1/2}, \tag{24}$$

$$2V_{2y} = W_3 + (2W_{2x}^2 + W_3^2)^{1/2}, \tag{25}$$

$$2V_{2z} = (2W_{2z}^2 + W_3^2)^{1/2} + (2W_{2x}^2 + W_3^2)^{1/2} - 2W_{2z}S_z. \tag{26}$$

In view of (20), the only parameters that need to be determined are W_2 and W_3. The value of S we estimate from the overlaps calculated by Gilbert *et al.*[13] to be 0.3. By using an angle $\phi = 144°$ (quartz), whereby $\theta = 18°$, we obtain values for all parameters by setting $2V_{2y} = 10.2$ eV and $2V_{2x} = 11.7$ eV according to our optical-excitation assignments. This is enough to determine our two fundamental parameters to be $W_2 = 10.75$ eV and $W_3 = 4.35$ eV. The resulting values for the other parameters are listed in Table II. In particular we note the values of the two internal polarities $\beta_{p_x} = 0.73$ and $\beta_{p_z} = 0.29$ which are measures of how polar the respective Si-O bonds are. For completeness we also define $\beta_{p_y} = 1$ denoting the fact that the p_y orbital does not interact at all with the neighboring Si hybrids.

Having determined W_2 and W_3 we can also evaluate all the parameters for angles other than $\phi = 144°$, which corresponds to quartz and amorphous silica (Table I). As an example, in Fig. 10 we plot the polarities β_{p_x} and β_{p_z} and in Fig. 11 the quantities V_{2y}, V_{2x}, and V_{2z} as functions of the Si-O-Si angle.

Perhaps even more interesting, we are also able to predict all the relevant parameters for GeO_2.

For the fundamental parameters W_2 and W_3 we are guided by the results of the bond-orbital model on simple tetrahedral crystals as follows. W_2, the bonding matrix element is of the same nature as V_2 of the tetrahedral crystals, which was found by Harrison and Ciraci[21] to vary as d^{-2} from material to material. This same d^{-2} dependence of similar matrix elements was subsequently found by Pantelides[34] to hold in ionic crystals of the rocksalt structure as well. We therefore assume a simple d^{-2} rule for W_2. From its value for SiO_2 we obtain

$$W_2 = 3.6(\hbar^2/m)d^{-2} . \quad (27)$$

For GeO_2, for which $d = 1.74$ Å, we obtain $W_2 = 9.13$ eV.

As for W_3, we use Eq. (14) and the fact that the hybrid energy[52] of Si is lower than that of Ge by 0.27 eV to obtain a value of $W_3 = 4.49$ eV for GeO_2. Using the observed angle $\phi = 130°$ for GeO_2 we then proceed to calculate all the other quantities of the model. They are listed in Table II along with those of SiO_2. In terms of these quantities, physical properties may be directly predicted. This was done, for example, for the optical-absorption spectrum, as mentioned in Sec. V, and will be done for other properties in the remainder of this paper.

Finally, we conclude this section with a note on how the band parameters of Sec. IV were determined. For the diagonal matrix elements one needs ϵ_{B_x}, ϵ_{B_y}, and ϵ_{B_z}. These are directly evaluated from Eqs. (21) and (22) by using the parameters of Table II. ϵ_y is used to set the zero of energy. For example, for β-cristobalite the result is $\epsilon_x = \epsilon_y$ and $\epsilon_z = \epsilon_x - 5.0$ eV. For the off-diagonal elements we need to evaluate V_p. We do this by noting that the top of the valence bands is at $\epsilon_y + V_p$ and the bottom at $\epsilon_z - 6B_1$, for a total width of $\epsilon_y - \epsilon_z + V_p + 6B_1$. By using the expression

$$B_1 = \tfrac{1}{4}(1 - \beta_{p_z})V_1 + \tfrac{1}{3}(1 + \beta_{p_z})V_p$$

and a value of $V_1 = 1.4$ eV from our previous results on Si,[27] we obtain the total width explicitly in terms of V_p and known parameters. The value of V_p is then determined to reproduce the observed total width in quartz, i.e., 11.3 eV.

VII. REFRACTIVE INDICES AND DIELECTRIC CONSTANTS

We turn now to the refractive index at long wavelengths, usually denoted by n, or, equivalently, the electronic dielectric constant ϵ_∞. The two are related by

$$n^2 = \epsilon_\infty . \quad (28)$$

In order to calculate an expression for the dielectric constant generally one starts by calculating the change in the electronic charge density caused by the application of an external potential. In the general formalism[53] this is done by calculating the changes in the occupied Bloch functions to first order in the applied field and summing over the Brillouin zone. The standard expression for ϵ_∞ is then

$$\epsilon_\infty = 1 + \frac{4\pi e^2\hbar^2}{m} \sum_{nk} \sum_{n'} \frac{f_{n'nk}}{(E_{n'k} - E_{nk})^2} , \quad (29)$$

where E_{nk} are the energy bands, n is summed over the occupied bands and n' over the empty bands, and the oscillator strength $f_{n'nk}$ is given by

$$f_{n'nk} = (2\hbar^2/m)\langle\psi_{n'k}|\nabla|\psi_{nk}\rangle^2/(E_{n'k} - E_{nk}) . \quad (30)$$

Here ψ_{nk} are the Bloch functions.

Clearly, this general formalism requires that one knows both the energy bands and Bloch functions over a sufficiently large mesh of points in the Brillouin zone. Moreover, the calculation, which in the end will yield one number, must be done numerically. In contrast, in our model, the bond-orbital approximation makes the calculation of ϵ_∞ a much simpler operation. We do not start with (29). Instead, we notice that, with the bond-orbital approximation, the total energy and charge density are given by the bond orbitals themselves, without a need for explicit Bloch functions and energy bands in k space. In particular, the total electronic energy is proportional to the sum of bond energies and the total charge density is proportional to the charge density of the bond orbitals (see Sec. III). Thus, for the dielectric constant calculation, one only needs to calculate the changes in the individual bond orbitals. This is equivalent to saying that the dielectric constant may be calculated by treating the crystal as a collection of polarizable bonds. Hence

$$\epsilon_\infty = 1 + 4\pi N_b \alpha_b , \quad (31)$$

where α_b is the bond polarizability and N_b is the density of bonds. [Equation (31) would apply in the case of the tetrahedral crystals where there is only one kind of bonds. In SiO_2, one must sum over the B_x, B_y, and B_z bonds; see below.]

Before we go on to how α_b is calculated, it is useful to compare this approach with analogous approaches to the dielectric constants of ionic crystals, such as the alkali halides. The classical approach[54] has been to treat the crystal as a collection of independently polarizable *ions* so that[55]

$$\epsilon_\infty = 1 + 4\pi(N_+ \alpha_+ + N_- \alpha_-) . \quad (32)$$

The polarizability of each species of ion has been thought to be independent of its environment. This approach has recently been criticized by Pantelides.[56] In fact it was shown[56] that the concept of independently polariable ions is invalid

and that the extreme opposite assumptions hold. This criticism does not apply to the assumptions leading to (31) for tetrahedral crystals and SiO_2. In fact it does not invalidate (32) either. Instead, the results of Ref. 56 could be summarized by saying that α_+ is in most cases negligible and α_- is not an intrinsic property of the *anion* but is rather determined by the cation and the interatomic spacing. In other words, one could still write

$$\epsilon_\infty = 1 + 4\pi N\alpha \ , \tag{33}$$

where N is the density of anions with α given by

$$\alpha = gCd^6 \ ,$$

where g is a geometric factor,[57] C is a constant that depends only on the *cation* and d is the interatomic spacing (see also Ref. 58).

Going back to (31), it remains to be seen how α_b is to be calculated. For tetrahedral solids, Harrison calculated α_b by simply calculating the dipole $\vec{P}$ induced in each bond by an external field $\vec{\mathcal{E}}$ whereby

$$\vec{P} = \alpha_b \vec{\mathcal{E}} \ . \tag{34}$$

Alternatively, it may be calculated by using the general quantum-mechanical formula for a localized system, namely[59]

$$\alpha_b = \frac{2e^2}{m} \sum_{jj'} \frac{\langle \phi_j | x | \phi_{j'} \rangle^2}{E_{j'} - E_j} \ , \tag{35}$$

where ϕ_j are the occupied orbitals and $\phi_{j'}$ are the available excited orbitals. This proves to be a simpler calculation in the case of SiO_2 and therefore we first see how it works for tetrahedral crystals.

For a bond in a tetrahedral crystal, ϕ_j is simply the bond orbital $|b\rangle$. By including only the antibonding orbital $|a\rangle$ in the sum over j', the calculation becomes very simple. The energy denominator is simply $2(V_2^2 + V_3^2)^{1/2}$ (notation of Refs. 18 and 21), while the matrix element may be expressed

$$\langle b|x|a\rangle = \tfrac{1}{2}\alpha_c(\langle h_a|x|h_a\rangle - \langle h_c|x|h_c\rangle) - \alpha_p\langle h_a|x|h_c\rangle \ , \tag{36}$$

where α_p is the polarity and α_c is the covalency given by

$$\alpha_c = (1 - \alpha_p^2)^{1/2} \ . \tag{37}$$

In Ref. 21, the second term in (36) is set equal to zero by assuming symmetrically disposed hybrids. By defining[21] the quantity in square brackets equal to $\frac{1}{4}\gamma a$, where a is the lattice spacing, as in Ref. 21, and substituting in (35) we get for the bond polarizability

$$\alpha_b = e^2\gamma^2 d^3 \alpha_c^2 / 6(V_2^2 + V_3^2)^{1/2} \ , \tag{38}$$

where d is again the interatomic spacing (bond length). Substituting this in (31) and using $N_b = \frac{1}{2}N$ (N is the density of electrons) we get Harrison's formula

$$\epsilon_\infty = 1 + [\gamma^2 \pi N e^2 d^2 / 3(V_2^2 + V_3^2)^{1/2}]\alpha_c^2 \ . \tag{39}$$

For the diamond-type crystals ($V_3 = 0$, $\alpha_c = 1$), this reduces to

$$\epsilon_\infty = 1 + \gamma^2 \pi N e^2 d^2 / 3V_2 \ . \tag{39'}$$

We turn now to the dielectric constant of SiO_2. The bond-orbital approximation again allows us to treat the crystal as a collection of polarizable bonds. Each "bond" now is, however, in effect three bonds (the B_x, B_y, and B_z bond orbitals) whereby the sum in (35) will give us at least three terms. By including only the three main excitations we identified in Sec. VI, namely $B_x \rightarrow A_+$, $B_y \rightarrow A_+$, and $B_z \rightarrow A_+$, the three energy denominators are $2V_{2x}$, $2V_{2y}$, and $2V_{2z}$, respectively (Fig. 3).

We now need the corresponding matrix elements. If we take $|A_+\rangle = |A_x\rangle$, then

$$|A_+\rangle = |A_x\rangle = [\tfrac{1}{2}(1 + \beta_{p_x})]^{1/2}|b\rangle - [\tfrac{1}{2}(1 - \beta_{p_x})]^{1/2}|p_x\rangle \ , \tag{40}$$

and the necessary matrix elements could be written in terms of $\langle b|x|p_x\rangle$, $\langle b|y|p_y\rangle$, $\langle b|z|p_z\rangle$, $\langle b|z|a\rangle$, and the center of gravity of each orbital, such as $\langle b|x|b\rangle$. In the simple tetrahedral solids the corresponding matrix elements were reduced to a single one by selecting the origin such that $\langle h_c|\vec{r}|h_a\rangle = 0$ and writing $\langle h_c|z|h_c\rangle - \langle h_a|z|h_a\rangle = \gamma d$. Thus γ would be unity if the hybrids were localized at the nuclear sites. We may see that this point of view is inadequate in SiO_2 by assuming localized orbitals leading to

$$\langle B_x|x|A_+\rangle \rightarrow -\tfrac{1}{2}(\beta_{c_x} d\sin\theta) \ , \tag{41}$$

$$\langle B_y|y|A_+\rangle \rightarrow 0 \ , \tag{42}$$

$$\langle B_z|z|A_+\rangle \rightarrow [(1 - \beta_{b_z})(1 + \beta_{p_x})]^{1/2}\tfrac{1}{2}(d\cos\theta) \ . \tag{43}$$

This point of view will provide a useful description when we describe the *change* in dipole with the movement of the atoms since the orbitals move with the atoms. However, Eq. (42) provides no coupling with the $|B_y\rangle$ mode though the optical properties (Sec. VI) show that such coupling is comparable to the others. The reason is quite clear: The orbital $|b\rangle$ included in $|A_+\rangle$ closely resembles the oxygen $|3s\rangle$ orbital [$\langle 3s|b\rangle \lesssim 1$; cf. Eq. (23)] and therefore has strong coupling with all three oxygen p orbitals. Assuming this is the dominant term, one is led to

$$\langle B_x|\vec{r}|A_+\rangle \rightarrow -\gamma' \beta_{p_x} \tfrac{1}{2}\vec{d} \ , \tag{44}$$

$$\langle B_y|\vec{r}|A_+\rangle \rightarrow \gamma'[\tfrac{1}{2}(1 + \beta_{p_x})]^{1/2}\tfrac{1}{2}d \ , \tag{45}$$

$$\langle B_z|\vec{r}|A_+\rangle \rightarrow \gamma'[\tfrac{1}{4}(1+\beta_{p_x})(1+\beta_{p_z})]^{1/2}\tfrac{1}{2}d\,, \qquad (46)$$

where $\gamma' \equiv 2\langle p_x|x|3s\rangle\langle 3s|b\rangle/d$ and is the same for y and z orientations. This form would of course not be useful in the displacing of atoms since the $|b\rangle$ orbitals move with the silicon atoms, not the oxygen atoms.

It is important to recognize that the terms of Eqs. (41)–(43) and Eqs. (44)–(46) are not additive contributions to the matrix elements but different parametrizations useful for different properties. The same differences would have arisen in the simple solids, had we looked at graphite rather than diamond structures. The localized orbitals picture would have remained appropriate for describing charge movement under distortion but would have missed the coupling of the π states with the antibonding bands under fields perpendicular to the layers.

Using Eqs. (44)–(46) the dielectric constant becomes

$$\epsilon_\infty = 1 + \frac{\pi N e^2 d^2 \gamma'^2}{9}\left(\frac{\beta_{p_z}^2}{V_{2x}} + \frac{1+\beta_{p_x}}{2V_{2y}} + \frac{(1+\beta_{p_x})(1+\beta_{p_z})}{4V_{2z}}\right). \qquad (47)$$

All quantities are known except γ' which may be fitted to the experimental value. A value of $\gamma' = 1$ in fact gives $\epsilon_\infty = 2.37$ for α-quartz, compared to the experimental 2.40.

We may expect γ' to be relatively insensitive to structure and can therefore predict the values of ϵ_∞ for the various forms of SiO_2 using values of N, d, and ϕ from Table I. These are compared with the experimental values in Table III. Good agreement is obtained in all cases except for β-cristobalite and coesite. This discrepancy may be understood by noting that β-cristobalite and coesite are the only forms for which ϕ is thought to deviate appreciably from 144°, the value in quartz. The results of Table III may therefore mean one of two things. γ' might have appreciable dependence on ϕ. On the other hand, it is likely that $\phi = 180°$ is unrealistic even for β-cristobalite. Taking $\phi = 144°$ gives us $\epsilon_\infty = 2.05$ in better agreement with the experimental value of 2.17. Similarly the value $\phi = 120°$ for coesite may be erroneous in view of the fact that the suggested structure does not agree with the observed density (see Ref. 28 and footnote b of Table III).

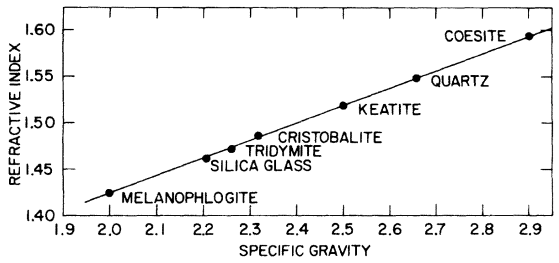

FIG. 12. Empirical correlation between the refractive index n of the various forms of SiO_2 and their respective specific gravities.

There exists an empirical linear correlation between the refractive index n, or, equivalently $(\epsilon_\infty)^{1/2}$ and the specific gravity of each of the forms of SiO_2. This is shown in Fig. 12, taken from Ref. 60. It is not altogether reliable, however. For example, when P. P. Keat[61] first grew crystals of what later was called keatite, he measured the index of refraction to be 1.513 ($\epsilon_\infty = 2.29$) and then used the empirical plot of Fig. 12 (*sans* keatite) to infer the specific gravity (density) of the new form of silica. In subsequent quotations of the plot (such as Ref. 60) this fact was not

TABLE III. The density of electrons N and theoretical and experimental (Ref. 63) values for the dielectric constants ϵ_∞ of the various forms of SiO_2 and GeO_2. The angular dependence of γ' has been neglected.

	Substance	N (Å^{-3})	ϵ_∞ (Theor.)	ϵ_∞ (Expt.)
SiO_2	α-quartz	0.3187	2.37	2.40
	β-quartz	0.3028	2.30	2.34
	α-cristobalite	0.2802	2.25	2.21
	β-cristobalite	0.2615	2.74	2.17
	β-tridymite[a]	0.2665	2.02	2.19
	Coesite[b]	0.3483 (0.3614)	2.04	2.56
	Keatite[a]	0.3011	2.29	2.31
	Vitreous silica	0.2573	2.11	2.10
GeO_2	Quartzlike	0.2977	2.89	2.92
	Vitreous germania	?	...	...

[a]We assued $\phi = 144°$ as in quartz.

[b]The value 0.3483 assumes 16 SiO_2 molecules per cell, according to the suggested structure. The measured density, however, points to 16.6 molecules per cell, whereby $N = 0.3614$ Å^{-3}.

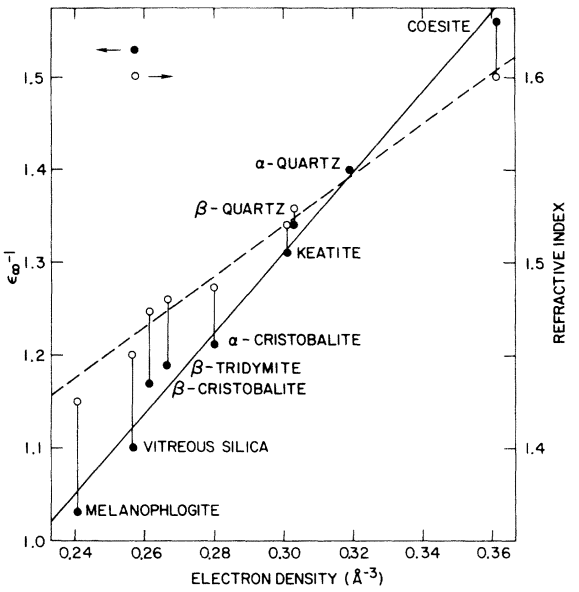

FIG. 13. Plot of $\epsilon_\infty - 1$ and also n against the electron density N for the various forms of SiO_2. Linear relationships are satisfied in both cases but theory predicts only the relation for $\epsilon_\infty + 1$. See text.

pointed out. It is not clear whether such interpolations were made for any of the other forms of silica. Another difficulty with Fig. 12 is that coesite is shown with specific gravity 2.9 whereas Coes[62] measured it to be 3.01.

In any case, it might be worth checking whether our formula for ϵ_∞, Eq. (47), can explain the origin of this empirical observation. We immediately observe that since d, the Si-O distance, is rather constant for the various forms (Table I) Eq. (47) yields

$$\epsilon_\infty = 1 + C(\theta)N\,, \tag{48}$$

where $C(\theta)$ is only a function of θ. The variation of θ is, however, also small and in fact the function $C(\theta)$, when evaluated, is found not to vary appreciably with θ. We would thus predict that, roughly

$$\epsilon_\infty - 1 = CN\,, \tag{49}$$

which is *not* the same as the empirical relation of Fig. 11, which may be expressed

$$(\epsilon_\infty)^{1/2} = C_0 + C'N\,. \tag{50}$$

However, Eq. (50) may be regarded as a linear fit to $(\epsilon_\infty)^{1/2} = (1 + CN)^{1/2}$, which appears to be adequate in the region of observed N's. To illustrate this we have plotted in Fig. 13 both $\epsilon_\infty - 1$ and $n = (\epsilon_\infty)^{1/2}$ against the electron density N (N is proportional to the specific gravity). The values of ϵ_∞ were taken from Ref. 63 and the values of N were calculated from the structural data listed in Table I (See Table III). It is clear from Fig. 12 that both (49) and (50) are rather well satisfied. Note that the solid line in Fig. 12 passes through the origin, as it should. The dashed line does not.

Finally, we attempt to predict ϵ_∞ for the quartz-like form of GeO_2. We use the parameters of Table II, $\gamma' = 1$ and evaluate Eq. (47). The result is $\epsilon_\infty = 2.36$. This number must, however, be corrected for the effect of d electrons which is Ref. 21 were included by multiplying γ by a factor 1.18. Using the same factor here we get a final value of $\epsilon_\infty = 2.89$ in excellent agreement with the experimental[63] value 2.92.

IX. TOTAL ENERGIES AND EFFECTIVE CHARGES

At this point we turn to examine a series of problems relating to effective charges on the atoms. The simplest case is the static effective charge which corresponds to the net charge on each atom in the unperturbed crystal. It generally involves some arbitrariness in the way it is defined but the tight-binding model we have been using provides a natural definition.[18,21,24,26] For example, for the simple bond orbitals $|b\rangle$ in zinc-blende-type crystals [Eq. (4)], it is natural to identify $|u_a|^2$ and $|u_c|^2$ as the fraction of each electron to be associated with the anion and cation respectively. The effective charge on each ion is then calculated in a straightforward manner to be

$$Z_a^* = 8|u_a|^2 - Z_a\,, \tag{51}$$

$$Z_c^* = 8|u_c|^2 - Z_c\,, \tag{52}$$

in units of the electron charge e. Here Z_a and Z_c are the formal valences of the anion and cation, respectively. Since $Z_a + Z_c = 8$ and[64] $|u_a|^2 + |u_c|^2 = 1$, we note that $Z_a^* + Z_c^* = 0$ or

$$Z_c^* = -Z_a^* = Z^*\,, \tag{53}$$

as it should.

As we saw in Sec. III, u_a and u_c were obtained by minimizing the bond energy $\langle b|H|b\rangle$, a step which, because of the bond-orbital approximation, corresponded to minimizing the total electronic energy. In view of (11), the result for zinc-blende-type crystals is

$$Z_a^* = -Z_c^* = 4\alpha_p - \Delta Z\,, \tag{54}$$

where $\Delta Z = Z_a - 4$.

The analysis for the static effective charges in SiO_2 and GeO_2 is now straightforward. We sum the contributions of all three bond orbitals B_x, B_y, and B_z and the result is

$$Z_0^* = \beta_{p_x} + \beta_{p_y} + \beta_{p_z} - 1 \tag{55}$$

or, since $\beta_{p_y} = 1$,

$$Z_0^* = \beta_{p_x} + \beta_{p_z}\,. \tag{56}$$

The value of this charge in SiO_2 (quartz) and GeO_2 is 1.02 and 1.05, respectively, as listed in Table II. For the various forms of SiO_2, Z_0^* is plotted as a function of the Si-O-Si angle in Fig. 10 in the approximation that W_3 does not depend upon θ. The values are in good agreement with those calculated by cluster methods.[13,14]

The static effective charges we just discussed do not enter experiments very directly, however. Any experimental measurement perturbs the system and the measured value contains contributions from the redistribution of charge caused by the perturbation. This, in turn, changes the value of W_3. The problem is fundamentally more difficult in SiO_2 than in the simple tetrahedral solids. In the latter, symmetry guarantees that there is no net change in the charge on an atom *linear* in displacement, whereas in SiO_2 there is. The algebra is rather involved and for simplicity we will first carry out the analysis for a simple tetrahedral solid. The generalization to SiO_2 will then be straightforward. In order to simplify the algebra even further we will neglect the small effects of the overlap S. The analysis is directed at the total energy and charge distribution as a function of local distortion; effective charges are only one aspect.

In simple bonds, the bond orbital was written as a linear combination of hybrids on the two atoms sharing the bond, $|b\rangle = u_a|h_a\rangle + u_a|h_c\rangle$. The matrix element of the Hamiltonian between any two hybrids was called $-V_2$ (or $-W_2$ for the corresponding situation in SiO_2). The difference in the expectation value of the Hamiltonian with respect to the two hybrids, was written $2V_3$ and the form of the bond orbital was obtained by minimizing the energy

$$\langle b|H|b\rangle = -(u_a^2 - u_c^2)V_3 - 2u_a u_c V_2 . \tag{57}$$

We now note that the energy difference $2V_3$ will shift with a change in effective charge and therefore itself depends upon u_a and u_c. We may incorporate this dependence explicitly in order to see more clearly the meaning of our empirically determined V_3 and to see how to include the effects of changing effective charges.

We write the value of V_3 which would be appropriate if all constituent atoms were neutral as V_3^0. We might estimate it from the difference in hybrid energies, calculated from the atomic term values; a value of 1.88 eV, for example, is found for GaAs. We then imagine transferring electrons to the nonmetallic atom, giving it extra charge and therefore changing the potential seen by an electron on that atom in proportion to the charge transferred, z. The magnitude of the corresponding reduction in V_3 is written $A_0 z\, e^2/d$, where d is the equilibrium bond length, introduced to make A_0 dimensionless. The $A_0 z e^2/d$ is taken to depend only on the atoms involved and independent of the positions of the atoms. This increase in energy is partially compensated by the lowering of the electron energy due to the neighboring atoms which are now positively charged. The magnitude of that correction is written $A_M z e^2/d$, where A_M is the familiar Madelung constant for the structure,[65] frequently written α_R, and does depend on the atom positions. This term is known; the constant A_M is 1.638 for the zinc-blende structure,[66] leading to a contribution to V_3 of 9.6 eV in GaAs. Comparison with the known value of V_3 = 1.21 eV in GaAs, yields an equilibrium value of $A_0 z e^2/d$ of 10.3 eV. Thus there is very strong cancellation between the two electrostatic terms; that is perhaps not surprising in view of the subtlety of the changes in charge distribution involved in the transfer charge in the polar solid. In the SiO_2 calculation we will in fact take A_0 and A_M equal in the equilibrium crystal structure, an approximation which would be reasonable here but which we would not make use of.

It is clear that the shift in V_3 due to charge redistribution is just what is traditionally called "screening." It is frequently treated on the basis of a dielectric constant, but is here considered on a microscopic level. If this calculation leads to charge accumulation and long-range fields, the polarization of the distant bonds may be included using the dielectric constant. That additional step will in fact not arise in the discussions here but would, for example, if we sought the Lyddane-Sachs-Teller splitting.[67]

It is convenient at this stage to rewrite the energy of Eq. (57) in terms of the atomic charges z introduced above rather than in terms of u_a and u_c. We first write the charge on the atom in terms of the contributions from the four bonds surrounding it and from the nuclear charge,

$$z = 4(u_a^2 - u_c^2) - \Delta Z , \tag{58}$$

where ΔZ is one for GaAs, two for ZnSe, and three for CuBr, etc. We then use also the normalization condition, $u_a^2 + u_c^2 = 1$, to solve for u_a and u_c and obtain the bond energy

$$\langle b|H|b\rangle = -\tfrac{1}{4}(z + \Delta Z)V_3 - [1 - \tfrac{1}{16}(z + \Delta Z)^2]^{1/2} V_2 . \tag{59}$$

We may write V_3 explicitly in terms of z,

$$V_3(z) = V_3^0 - (A_0 - A_M)e^2 z/d . \tag{60}$$

To obtain the total energy we may sum the bond energies, Eq. (59), but subtract the Coulomb energies which have been counted twice, as usual in a self-consistent-field theory, and add Coulomb interactions between atoms. This yields the total

energy per atom pair (eight times the energy per electron) of

$$E_{\text{tot}} = -2zV_3^0 + (A_0 - A_M)z^2e^2/d - 8V_2[1 - \tfrac{1}{16}(z + \Delta Z)^2]^{1/2} . \quad (61)$$

This is the quantity to be minimized with respect to z to obtain the equilibrium effective charge and equilibrium energy.

A simpler way of obtaining this expression, which will be used when we go to SiO_2, is to integrate the work done in transferring charge between atoms, starting from neutral atoms,

$$-\int 2V_3(z)\,dz , \quad (62)$$

which yields the first two terms in Eq. (61). We then add the covalent energy $E_2(z)$ which is defined to be the *last term* in Eq. (61); it came directly from the last term in Eq. (57). This gives the same result.

Taking the derivative with respect to z we see that indeed the V_3 evaluated from Eq. (60) at the z corresponding to minimim energy plays the role of the polar energy V_3 in the simple theory and is the quantity fit to experiment, and that the value of z which minimizes the energy is $Z^* = 4V_3/(V_2^2 + V_3^2)^{1/2} - \Delta Z$ as in the simple theory [Eq. (54)].

Of particular interest here is how the charges and energies change when the system is distorted. We consider some distortion parameter η, which might be a particular shear strain, for example. The expression above for E_{tot} remains appropriate, but now A_M and V_2 become explicit functions of η. E_{tot} is a function of the two independent variables, η and z. In Fig. 14 we show a schematic contour plot of $E_{\text{tot}}(\eta, z)$ appropriate to η as a shear strain. For fixed η we may minimize with respect to z to obtain effective charges and the energy of the state. We may also minimize with respect to η to obtain the equilibrium η, which will be at $\eta = 0$ if η is a shear strain.

To compute the elastic shear constant we note that both A_M and V_2 vary only quadratically with η so Z^* also varies only to second order in η, and since at equilibrium E_{tot} is stationary with respect to z, we may obtain the change in energy, to second order in η, in terms of $\partial^2 E_{\text{tot}}/\partial\eta^2$ at constant z. This is also apparent from Fig. 14. There are two contributions: the first, from $\partial^2 A_M/\partial\eta^2$, is just the electrostatic contribution from fixed charges of Z^*. (Note $\partial^2 Z^*/\partial\eta^2$ does not enter.) The second, from $\partial^2 V_2/\partial\eta^2$, is just the contribution calculated by Harrison and Phillips,[22] who ignored electrostatic effects. The Madelung contribution to the elastic shear constant has been calculated by Blackman[68] and discussed by Martin.[69] The contribution to $c_{11} - c_{12}$

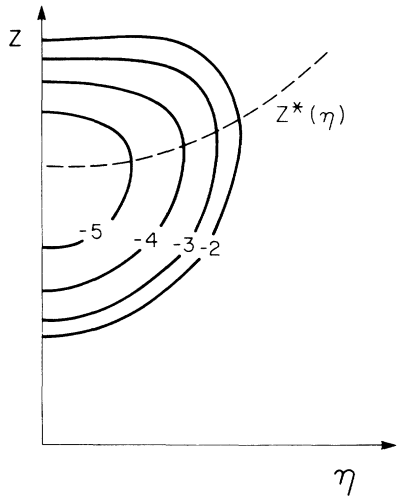

FIG. 14. Schematic contour plot of the total energy of a tetrahedral solid as a function of shear strain η and effective charge z. At any given strain, the ground state is obtained by minimizing the energy with respect to z. This leads to values $Z^*(\eta)$ indicated by the dashed line, which crosses each contour at the vertical tangent. According to this plot the effective charge would increase in proportion to the square of the shear; the elastic shear constant itself can be computed using the equilibrium effective charge $Z^*(0)$.

is given by $0.053\,Z^{*2}e^2/d^4$. In GaAs, for example, with $Z^* = 1.0$, the electrostatic contribution is 0.34×10^{11} erg/cm^2, very small compared to the experimental 6.5×10^{11} ergs/cm^2. Thus this generalization does not significantly affect the findings of Harrison and Phillips. Similarly, the effective transverse charges and piezoelectric charges[24] concerned changes linear in strain and are not at all affected.

The situation in SiO_2 is analogous. We have defined W_3 to be half the energy per electron in transferring charge from Si hybrids to O p states at the equilibrium positions and charge distributions. We now decompose this into a value W_3^0 appropriate to the neutral atoms and a term $-(A_0 - A_M)ze^2/d$, where z is the effective charge on the oxygen (or half the effective charge on the silicon) and d is the equilibrium Si-O distance. Thus we define a charge-dependent W_3 given by

$$W_3(z) = W_3^0 - (A_0 - A_M)ze^2/d . \quad (63)$$

The value we have fit to experiment is $W_3(Z^*)$, where Z^* is the value of z which minimizes the total energy.

To obtain the total energy explicitly we may, as in the tetrahedral solid, compute the work done in transferring charge, starting from the neutral atoms, $-\int 2W_3(z)\,dz$, and adding a covalent contribution E_2 which is the appropriate generalization

of the expression in the tetrahedral solids. It is convenient to divide the total energy by the number of oxygen atoms to obtain what we call the energy per bonding unit,

$$E_{\text{tot}} = -2z\,W_3^0 + (A_0 - A_M)z^2e^2/d + E_2(z)\ . \qquad (64)$$

The energy E_2 actually depends on the coefficients in the wave functions for both the states B_x and B_z, but for fixed z we will use the forms of B_x and B_z which minimize E_2 and therefore can discuss E_2 as a function of z only. We see from Eqs. (18)–(22) that the contributions from $\langle B_x|H|B_x\rangle$ and $\langle B_z|H|B_z\rangle$ are $-\sqrt{2}(1-\beta_{p_x}^2)^{1/2}W_2\sin\theta$ and $-\sqrt{2}(1-\beta_{p_z}^2)^{1/2}W_2\cos\theta$, respectively. Adding the contributions from both spins, the energy for the bonding unit, consisting of the oxygen and the two silicon hybrids from its neighbors, is

$$E_2 = -2\sqrt{2}\,W_2[(1-\beta_{p_x}^2)^{1/2}\sin\theta + (1-\beta_{p_x}^2)^{1/2}\cos\theta]\ . \qquad (65)$$

As a simple check we may substitute this in Eq. (64) for the case when $A_0 = A_M$. Then substituting the equilibrium values of β_{p_x} and β_{p_z} from Eqs. (18) and (19) we obtain the equilibrium energy corresponding to Eqs. (21) and (22).

We may recall, however, that the charge z on the oxygen is given by [Eq. (56)]

$$z = \beta_{p_x} + \beta_{p_z}\ . \qquad (66)$$

Then $E_2(z)$ is the value of Eq. (65) which minimizes it subject to the condition, Eq. (66). Taking the derivative of Eq. (64) with respect to z confirms the fact that $W_3(Z^*)$, from Eq. (63), plays the role of the W_3 in the simple theory and that in fact the equilibrium value of Z^* is given by Eq. (66).

We will need the Madelung constant A_M which could be calculated for any structure using Ewald methods.[70] Of more direct use here is an approximate calculation which will serve for all SiO_2 structures. A_M has been defined such that the electrostatic potential at an oxygen atom due to all of its neighbors minus the potential at a silicon atom, due to all of its neighbors, is $2A_M(-ze)/d$. Here $-ze$ is the charge on the oxygens ($+2ze$ is the charge on the silicons) and d is the silicon-oxygen distance. Kittel[71] has described a way of estimating such potentials by summing over groups of atoms which have net neutrality, noting that such estimates converge rapidly and meaningful estimates can be made for small groups. The groups we choose are shown in Figs. 15(a) and 15(b). The electrostatic potential can be written down immediately by inspection, $(4-\sqrt{\frac{27}{8}})ze/d - (-4+1/\cos\theta)ze/d$, corresponding to a Madelung constant of

$$A_M = 3.1 - 1/(2\cos\theta) \qquad (67)$$

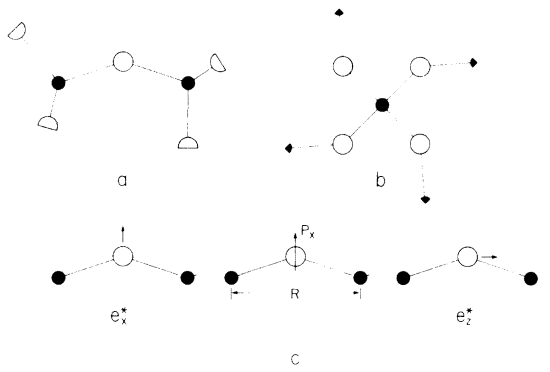

FIG. 15. (a) Neutral group used to obtain the electrostatic potential at an oxygen atom, shown as a large circle. The group also includes two silicon atoms, at twice the oxygen charge, $2z$, and the six oxygen neighbors completing the silicon tetrahedra; each of these is counted as of charge $\frac{1}{2}z$. For silicon the group (b) is used, including four oxygen neighbors and each of those oxygens' other neighbors, each counted as $\frac{2}{4}z$. (c) Three distortions of the bonding unit which are discussed in the text.

or 2.6 for SiO_2 (quartz). Some measure of the accuracy can be given by, for example, extending the group for the silicon potential by completing the four outer silicons in Fig. 15(b) and adding the three neighboring oxygens to each, with each added oxygen counted as charge $\frac{1}{2}z$. If these three are concentrated at their center of gravity, the correction to A_M for SiO_2 is $+0.24$.

We have obtained values of W_2 and the equilibrium W_3 from fitting the spectra. If we estimate W_3^0 from the atomic term values, as we did in the tetrahedral solids, we obtain a value $W_3^0 = 2.93$ eV, for SiO_2 in comparison to the experimental $W_3 = 4.35$ eV and our estimated $A_M Z^* e^2/d$ of 24 eV. As in the tetrahedral solids the large electrostatic terms very nearly cancel each other, but in this case the Madelung term appears slightly larger. This is surprising, though not inconceivable. The estimates are somewhat uncertain in any case and we choose here for simplicity to take A_0 equal to A_M in the equilibrium structure (and thus W_3^0 equal to the equilibrium W_3). This does not affect our results in an important way and provides us with definite values for all parameters in the problem as well as a procedure for extending the calculation to all systems.

We are now prepared to address specific properties. The first, and perhaps most important, class of properties we will consider concerns the variation of the bond angle at oxygen. We will address both the energetics involved in changing the bond angle and effective charge questions.

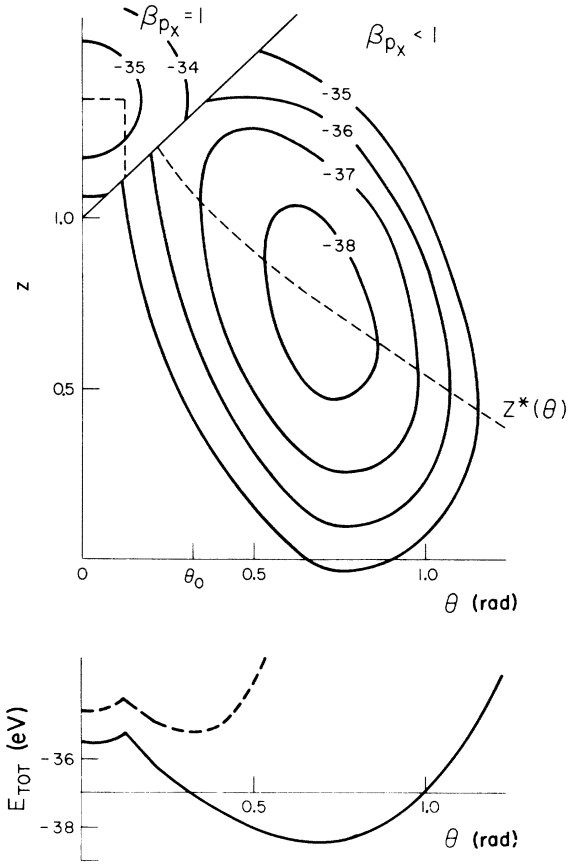

FIG. 16. Total energy in SiO_2 (in electron volts per bonding unit consisting of a single oxygen atom and the two silicon hybrids with which it bonds) shown above as a contour plot as a function of bond angle at the oxygen and the effective charge z on the oxygen. The dashed line Z^* gives the effective charge in the ground state as a function of angle as in Fig. 14. (Cf. with curve in Fig. 10.) θ_0 is the equilibrium angle. The behavior at small angles and high charge is qualitatively different; analytic continuation from the other region yields β_{px} greater than one, which is unphysical. The region above the corresponding phase boundary has not been explored carefully though it may be essential to an understanding of the transition to any high-temperature phase of SiO_2 in which θ is zero. The lower curve is a plot of the minimum energy as a function of θ. The dashed line is obtained by adding the R^{-12} interaction between silicons discussed in the text.

A. Variation of the bond angle at the oxygen

The covalent contribution to the energy, given in Eq. (65), is minimized when the bond angle at the oxygen is 90° (i.e., $\theta = 45°$). It has long been understood that such contributions are the origin of the asymmetric position of the oxygen atoms between the silicon atoms. We thought initially that the observed angle near 144°, rather than 90°, came from the electrostatic term, the A_M term in Eq. (64); this term tends to keep the silicon atoms apart, opening up the silicon angle. We will see, however, that that term is much too small.

We may make this quantitative using the total energy given in Eq. (64). We have taken A_0 equal to A_M at the equilibrium angle so that at fixed Si-O distance the second term in Eq. (64) becomes simply $+z^2e^2(1/\cos\theta - 1/\cos\theta_0)/2d$, where θ_0 is the equilibrium angle, [see Eq. (67)] and W_3^0 is the value of W_3 given in Table II. E_2 is evaluated from Eq. (65) by minimizing it as we have described. A contour plot of the resulting energy is shown in Fig. 16, analogous to the corresponding plot for the tetrahedral solids in Fig. 14.

We see immediately that the minimum occurs near 40° ($\theta = 0.7$ rad), in poor agreement with the experimental 18°. Though the electrostatic interaction has been included it has only opened up the oxygen angle a few degrees. We may look back at what has been omitted in the calculation. The change in W_{2x} and W_{2z} [Eq. (20)] due to the $\sin^2\theta$ or $\cos^2\theta$ in the denominator is a tiny effect. The contributions from the first terms in Eqs. (21) and (22) are proportional to $\sin^2\theta$ and $\cos^2\theta$ and, when added, are independent of angle. The matrix element between the two silicon hybrids, which we have neglected, can be estimated from the atomic matrix elements and separation dependence[27] to be about 1 eV; it enters by effectively decreasing the W_3 entering the B_x by $\frac{1}{2}$ eV and increasing the W_3 entering B_z by the same amount. Its effect on the total energy is very small.

However, the direct repulsion between the silicon atoms due to the overlap of the electron densities may be appreciable. This is the contribution which dominates inert gas interactions where no bonding occurs; it is also the zero-order interaction between silicon atoms to which we have found the bonding corrections. We note that in SiO_2 the Si-Si distance is 3.06 Å, only 30% larger than the separation in pure silicon. We note also that the spacing in solid argon is 3.76 Å; it is determined by the overlap interaction between atoms which we might expect to be more compact than silicon due to the additional nuclear charge. A study of this overlap interaction in open-shell systems is in progress and will be reported elsewhere. Here we simply introduce an R^{-12} repulsion of the usual form[72] and see that it could account for the observed properties. We write the overlap interaction between a pair of silicon atoms separated by R in the form $U_0(R_0/R)^{12}$, where R_0 is the separation 3.06 Å observed in SiO_2. U_0 is adjusted such that this term, added to the E_{tot} of Fig. 16, gives the observed equilibrium angle; the value obtained is $U_0 = 1.68$ eV. Thus only a relative weak interaction is required to bring the

calculated angle into agreement with experiment.

We may next look at the angular rigidity, associated with the second derivative of the total energy with respect to angle, which may be derived from the lower curve of Fig. 16. It is remarkable that though $d^2E_{tot}/d\theta^2$ is large at the minimum (at $\theta = 0.7$ it equals 30 eV), it becomes smaller and finally negative at smaller θ (taking the value -4.5 eV at the observed angle, $\theta = 0.31$). The reason for this is essentially that given by Kleinman and Spitzer[73] in explaining a small or negative angular force constant for this distortion in quartz; the bond energy is a minimum at $\theta = 45°$ and a maximum at $\theta = 0$ and the inflection may be expected near the observed angle. However, the overlap interaction we have introduced above, which gives the correct equilibrium angle, has a second derivative with respect to angle of $12\ U_0$ $(13\tan^2\theta + 1) = 48$ eV at the observed angle. The experimental situation is not so clear. Kleinman and Spitzer[73] could fit their data as well with values between -21 and $+6$ eV. There is of course considerable uncertainty in our estimate due to the assumed form of the overlap interaction. It seems unlikely that this will be cleared up without a complete study of the overlap interaction. We might mention one other omission from our calculation, the correlation energy. However, an estimate of this effect, in analogy with the treatment of the corresponding term in the tetrahedral solids[21] suggests that the angular-dependent part (the interbond term) is small though it does favor small θ.

These additional terms in the total energy do not affect the value of Z^* at given θ and so we may proceed with a treatment of effective charges with more confidence. In particular, the values of 1.02 for oxygen in SiO_2 and 1.05 in GeO_2 can be regarded as meaningful. Similarly the change in effective charge with angle can be calculated. We could read the value of $\partial Z^*/\partial\theta$ from the slope of the dashed curve in Fig. 16 or can obtain it by differentiation of Eq. (66). The latter leads to

$$\frac{\partial Z^*}{\partial\theta} = \beta_{p_x}(1-\beta_{p_x}^2)\left(\frac{1}{W_3}\frac{\partial W_3}{\partial\theta} - \cot\theta\right) + \beta_{p_z}(1-\beta_{p_z}^2)\left(\frac{1}{W_3}\frac{\partial W_3}{\partial\theta} - \tan\theta\right); \qquad (68)$$

$$\frac{\partial W_3}{\partial\theta} = \frac{-Z^*e^2\sin\theta}{2d\cos^2\theta}$$

or -1.57 eV for SiO_2 and -2.28 eV for GeO_2. All other values are given in Table II leading to $\partial Z^*/\partial\theta$ of -1.33 for SiO_2 and -1.26 for GeO_2. These are large changes; physically their origin may be understood as the tendency of the silicon atoms to become more neutral (by drawing electrons to them) when they are brought closer together.

B. Arbitrary lattice distortions

We have considered the variation in energy as the bond angle at the oxygen is modified. The energy will of course also change when the bond length between adjacent silicon and oxygen atoms changes and, as in the tetrahedral solids,[22,24] this contains contributions to the energy other than the bonding terms we have considered. Kleinman and Spitzer[73] have fit the vibration spectrum using a radial force constant for this interaction corresponding to a change in energy of the bond of $\frac{1}{2}C_0(\delta d/d)^2$. Fitting this to the highest frequency vibrational mode led to a value of $C_0 = 70$ eV, comparable to the corresponding values in the simple tetrahedral solids (e.g., 70 eV for diamond and 55 eV for silicon obtained from the bulk modulus). This arises from the kind of overlap interaction mentioned above but not treated explicitly. They also introduced a force constant giving a change in energy due to a change in angle between two bonds measured at the silicon, $\frac{1}{2}C_1(\delta\phi)^2$, to be summed over all such angles. They could fit the vibrational spectra reasonably well with a C_1 in the range 3.9–6.3 eV. A full calculation of the energy in terms of our model would lead to a more complicated set of force constants than that assumed by Spitzer and Kleinman; however, we could treat the change in energy due to a particular distortion as Harrison and Phillips treated the shear constant in the simple tetrahedral solids.[22] This would require the addition of another scaling parameter λ of order 1. This does not seem fruitful until a full consideration of a range of materials is made.

We can, however, treat the effective charges which arise under various distortions of the bonding unit. We will define effective charges by taking our origin of coordinates at the midpoint between the two silicon atoms, computing the electric dipole induced under a given distortion, and defining the effective charge to be the fixed charge on the oxygen which would produce the same dipole under the same distortion. This is a natural generalization of the definition of effective charges in the simple tetrahedral solids, and has the advantage that it does not depend upon how charges are associated with the silicon atoms or silicon hybrids.

There are three atom positions required to specify the distortion of the unit. This corresponds to nine degrees of freedom, but the three uniform translations are not of interest. Three are pure rotations and therefore correspond to effective charges equal to the equilibrium charges Z^* which we have discussed previously. Two

correspond to displacements of the oxygen in the z direction or in the x direction while the silicons remain fixed, and one corresponds to moving the two silicons apart while the oxygen remains fixed. Displacement of the oxygen in the y direction is a pure rotation so we call the rotational charge e_y^*. It equals Z^*.

We consider next the displacement of the oxygen in the x direction. We write the magnitude of the displacement u and write the change in dipole due to the displacement of the atom and due to the corresponding changes in Z^*. This change in dipole is given by

$$\delta p_x = -eZ^*u - ed\sin\theta\left(\frac{\partial Z^*}{\partial d}\,u\sin\theta + \frac{\partial Z^*}{\partial\theta}\,\frac{u}{d}\cos\theta\right), \quad (69)$$

from which we immediately extract the effective charge $e_x^* = \delta p_x/(-eu)$. We could have inserted a factor γ of order unity in the second term of Eq. (69) in analogy with the corresponding factor in tetrahedral solids. This γ would be the factor required to make the relations (41)–(43) proper equalities. It could be adjusted to take into account asymmetries in the charge distributions. We chosen instead $\gamma = 1$ so that unambiguous effective charges can be obtained and then compared directly with experiment. The change in Z^* with θ (at constant d) was given in Sec. IX A. The change in d (at constant θ) comes through the change in W_2 and the change in W_3. Differentiating Eq. (66) gives

$$\frac{\partial Z^*}{\partial d} = [\beta_{p_x}(1-\beta_{p_x}^2) + \beta_{p_z}(1-\beta_{p_z}^2)] \times \left(\frac{1}{W_3}\,\frac{\partial W_3}{\partial d} - \frac{1}{W_2}\,\frac{\partial W_2}{\partial d}\right). \quad (70)$$

W_3 depends upon d through the Madelung term and is given by

$$\frac{d}{W_3}\frac{\partial W_3}{\partial d} = \frac{A_M Z^* e^2}{W_3 d}.$$

(Note that the change in Z^* did not contribute to the change in W_3 since A_M was taken equal to A_0; note also that $A_0 e^2/d$ was taken independent of d.) W_2 is taken to vary as d^{-2} as in the tetrahedral solids so $(d/W_2)\partial W_2/\partial d = -2$. Substituting numbers from Table II into Eq. (70) gives $(d/Z^*)\partial Z^*/\partial d$ equal to -1.95 for both SiO_2 and GeO_2. The effective charge

$$e_x^* = Z^* + d\,\frac{\partial Z^*}{\partial d}\sin^2\theta + \frac{\partial Z^*}{\partial\theta}\sin\theta\cos\theta \quad (71)$$

takes the values given in Table IV.

Similarly if each silicon is displaced by u away from their center of gravity, the change in dipole is

$$\delta P_x = -ed\sin\theta\left(\frac{\partial Z^*}{\partial d}\,u\cos\theta - \frac{\partial Z^*}{\partial\theta}\,\frac{u}{d}\sin\theta\right). \quad (72)$$

For this deformation it is convenient to write the ratio of the change in dipole moment to the dipole moment itself $(-Z^*ed\sin\theta)$ in terms of the fractional change in the silicon-silicon distance R:

$$\frac{R}{P_x}\left(\frac{\partial P_x}{\partial R}\right) = \frac{d}{Z^*}\left(\frac{\partial Z^*}{\partial d}\right)\cos^2\theta - \frac{1}{Z^*}\,\frac{\partial Z^*}{\partial\theta}\cos\theta\sin\theta\,; \quad (73)$$

values for this dimensionless constant are given in Table IV.

TABLE IV. Oxygen effective charges (in units of electron charges).

	SiO_2	GeO_2	KS Model (SiO_2)
e_x^*	0.45	0.21	0.93
e_y^*	1.02	1.05	1.50
e_z^*	2.74	2.54	−3.93
$\frac{R}{P_x}\frac{\partial P_x}{\partial R}$	−1.37	−1.15	−3.62

Finally we turn to the charge e_z^*. The evaluation is straightforward but a little more complicated. There is no change in W_3, by symmetry and as in simple tetrahedral solids, but we expect W_2 to vary as d^{-2} when the Si-O distances are changed. The simplest way to compute the charge is to consider a distortion in which one Si-O bond length is shortened by δd and the other is lengthened by δd with no change in angle. If we then add a rigid rotation around the oxygen (by an angle $\delta d\tan\theta/d$) and a rigid displacement (by $\delta d/\cos\theta$), we are led to the displacement corresponding to the charge e_z^* shown in Fig. 15 (with magnitude of displacement $\delta d/\cos\theta$).

The first step gives the charge transfer due to distortion. The increase in W_2 in the right-hand Si-O bond is $-2W_2\delta d/d$; W_2 decreases on the left. We treat these changes in matrix element as a perturbation and construct the perturbed states $|B_x\rangle$ and $|B_z\rangle$. The matrix element, for example, between $|B_z\rangle$ and the antibonding state $|A_x\rangle$ is directly obtained using the form of the states from Eqs. (17) and (40). We obtain

$$\langle A_x|H|B_z\rangle = (1-\beta_{p_x})^{1/2}(1-\beta_{p_z})^{1/2}\langle p_x|H|a\rangle - (1+\beta_{p_x})^{1/2}(1+\beta_{p_z})^{1/2}\langle b|H|p_z\rangle, \quad (74)$$

with $\langle p_x|H|a\rangle = \sqrt{2}\sin\theta\,2W_2\,\delta d/d$ and $\langle b|H|p_z\rangle = \sqrt{2}\cos\theta\,2W_2\,\delta d/d$. This gives $\langle A_x|H|B_z\rangle = -16 \times \delta d/d$ eV. Similarly, the matrix element between $|B_z\rangle$ and $|A_z\rangle$ vanishes for this distortion. The matrix element $\langle A_z|H|B_x\rangle$ turns out to be less than

a volt and so the distortion of the B_x state is negligible. The energy difference between $|B_z\rangle$ and $|A_x\rangle$ is

$$E_{ab} = (W_3^2 + 2W_2^2)^{1/2}\sin^2\theta + (W_3^2 + 2W_2^2)^{1/2}\cos^2\theta$$

or 18.4 eV. Thus the perturbed state may be written immediately, $|B_z\rangle - |A_x\rangle\langle A_x|H|B_z\rangle/E_{ab}$. This may be squared and the term in the probability density for the right-hand silicon hybrid, linear in displacement, is seen to be

$$-(1-\beta_{p_z})^{1/2}(1+\beta_{p_x})^{1/2}\langle A_x|H|B_z\rangle/2E_{ab} \qquad (75)$$

or 0.48 $\delta d/d$. The corresponding charge has been transferred a distance $2d\cos\theta$; we sum over both spins to obtain a dipole 1.83 $e\delta d$. To relate this to the effective charge we return to the deformation shown in Fig. 15 for e_z^*. The displacement δz gives a $\delta d = \delta z\cos\theta$. The induced dipole given above, which arises from the distortion alone, is $1.83e\delta z\cos\theta$ contributing 1.74 electrons to e_z^*. This is to be added to the Z^* obtained from direct displacement. The result is given in Table IV, along with the corresponding result for GeO_2; in that case, the deformation of the state $|B_x\rangle$ contributed 20% as much as that of $|B_z\rangle$ and was included. These effective charges enter a number of properties. Unfortunately the treatment of each property is complicated considerably by the complexity of the SiO_2 structure. We consider two properties for which sufficient theoretical work has been done to allow a reasonably direct comparison.

C. Piezoelectricity

For the microscopic theory of piezoelectricity in any system one must first learn how the atoms move relative to each other under elastic strain and must then compute the charge redistribution under that distortion. The first attempt at such a theory for quartz was made by Gibbs[74] in 1926 without any real knowledge of either of these aspects. He assumed that the silicon atoms moved as points in an elastic continuum (though there could in fact be internal displacements between the three silicon atoms in the primitive cell), that the Si-O bond distances remained fixed (though we have seen that the radial force constant C_0 is not all that much larger than the angular constants C_1) and that the angle which the plane of the bonding unit makes with the c axis does not change (presumably because that was a simple choice). He then assumed fixed charges $-eZ^*$ of each oxygen (and of course $2eZ^*$ on each silicon). The value of Z^* could then be fixed in terms of one of the measured piezoelectric constants; he obtained a value of $Z^* = 0.5$ using the piezoelectric constant e_{11}. This was recalculated by Machlup and Christopher[75] who obtained a value 0.34 from a presumably equivalent calculation. Had they used the other independent constant, e_{14} they would have obtained $Z^* = 0.05$.

Clearly the model is grossly inaccurate. We have not attempted a more realistic treatment of the deformation but we may use the effective charges obtained in the last section to rectify the error in the use of a rigid charge, at least in the context of the same model for the deformation. We will find that this does not improve the results and thus suggests that it is the model of the deformation which is at fault.

In the model used by Gibbs and by Machlup and Christopher (we have followed the work of the latter) there is no change in bond length so that the charges e_x^* and e_z^* do not provide the simplest description. It is most useful to proceed directly with Z^* and $\partial Z^*/\partial\theta$.

We may compute the effect of the corresponding charge transfer by considering each bonding unit. We write the vector distance between the two silicon atoms $\vec{R}$. For a strain $\epsilon_1 = \epsilon_{xx}$, the change in R is given by $\epsilon_1 R_x^2/R$, changing θ by $-\epsilon_1 R_x^2/2dR\sin\theta$. This gives a change in the x component of the dipole due to this effect of $(-\epsilon_1 R_x^2/2R)\partial Z^*/\partial\theta$, which may be summed over each bonding unit to obtain the contribution to e_{11} and to e_{14}; all of the necessary parameters have been given by Machlup and Christopher.

We note first that since Machlup and Christopher found a value of Z^* of 0.34 fit the experimental e_{11}, our use of 1.02, before making the transfer corrections, leads to an e_{11} a factor of three too large. We find that the transfer corrections increase this another 50%, worsening the discrepancy. Similarly the transfer corrections increase the error in e_{14} from a factor of 20 to a factor of 30. As we indicated earlier, the error seems to be in the deformations themselves. In that regard, it is of interest to note that though the transfer acts to reduce the dipole change, in the above calculation it increases the piezoelectric constant. The reason is that the contribution to the dielectric polarization (for both types of strain) arising from angular deformation of the Si-O-Si units is of opposite sign (and about half as big) as that due to rotation of the bonding units. Because of this cancellation the arbitrary assumption of fixed angle between the plane of the bonding unit and the c axis looks particularly suspect.

D. Infrared absorption intensities

The coupling between light and the lattice vibrations arises directly from the dipole moments induced by the vibrational distortion of the lattice. Given the form of the normal modes it is possible to calculate the coupling directly from the effective charges given in Table IV. This is

a very major undertaking even given the form of the modes and we will instead make a comparison using a model of the coupling introduced by Kleinman and Spitzer[73] (KS). They introduced a direct charge $-eZ^*$ ($-\frac{1}{2}eq$ in their notation) on the oxygen, and of course $2eZ^*$ on the silicon. They also recognized that there will be transfer charges (which they called valent charges) which they represented by a one-parameter diadic of the form $eQ\sum_\alpha \vec{\rho}_\alpha \vec{\rho}_\alpha$. Here the sum is over unit vectors $\vec{\rho}_\alpha$ from each oxygen atom to its nearest-neighbor silicon atoms. The contribution to the silicon charge is of opposite sign and summed over the four oxygen neighbors.

It is interesting that this model is not general enough to represent our calculated charges; it does not include the counterpart of $\partial Z^*/\partial\theta$. We may write the effective charges we have discussed in terms of the model of Kleinman and Spitzer,

$$e_x^* = Z^* - 2Q\sin^2\theta\ , \quad e_y^* = Z^*\ ,$$
$$e_z^* = Z^* - 2Q\cos^2\theta\ , \tag{76}$$
$$\frac{R}{p_x}\frac{\partial p_x}{\partial R} = -\frac{2Q\cos^2\theta}{Z^*}\ .$$

Comparison with the values we have predicted in Table IV makes it immediately clear that no reasonable fit can be made; e_y^* cannot in the model be made to be intermediate between e_x^* and e_z^*.

They nevertheless were able to fit the observed infrared absorption intensities. We may see how this was accomplished by substituting their values, $Z^* = 1.5$ and $Q = 3$, in Eq. (76) to obtain the values listed in the last column of Table IV. First we note that in the deformations corresponding to the three effective charges, the oxygen moves with respect to the silicons which is characteristic of optical modes; the bottom entry on the other hand corresponds to a relative motion of the silicons with the oxygen stationary with respect to their center of gravity which is characteristic of the acoustical modes and not relevant to the infrared properties. Furthermore the intensities depend upon the square of the effective charges and are therefore independent of the sign. We then see that Kleinman and Spitzer obtained the right ordering of the *magnitudes* by selecting parameters such that e_z^* was negative; there is no other way within the context of the model. It seems clear that our signs must be correct and the values from the model quite artificial. We may nevertheless use their model to test the prediction of the intensities based upon our charges.

About the best fit of our values using their model is with $Z^* = 1$ and $Q = 2$. This gives (compared with our values) 0.62 (0.45), 1 (1.02), and -2.62 (2.74) for the three charges. But these values of Z^* and Q are just $\frac{2}{3}$ the ones they obtained as a best fit. Thus our values would lead to exactly the same relative intensities which they *fit*, but would give absolute intensities too small by a factor of $\frac{4}{9}$. An absolute error in these intensities from a microscopic theory may not be surprising, and we find the agreement on the relative intensities most gratifying. Adjustment of the parameter γ could presumably improve the accord with experiment.

X. CONCLUSIONS

In this paper we have constructed a model in terms of which the electronic structure and a variety of properties of silica and germania may be studied in a comprehensive way. Some of the basic aspects of the model are definitely not new. For example, several authors[8-11] have in the past employed sp^3 hybrids on the silicons to describe the bonds in SiO_2. We have carried those simple, rather qualitative ideas farther and have been able to describe quantitatively not only energy levels and spectra but also the dielectric constants, elastic constants, and effective charges. All this was done with a minimum of computer calculations.[76] Instead the analysis was carried out analytically so in the end we were able to express most quantities as simple analytical functions of structural parameters (such as the Si-O-Si angle and Si-O distance) and two fundamental parameters, W_2 and W_3. This permitted a study of the various properties in the different allotropic forms of SiO_2.

Nevertheless, this paper, lengthy as it is, is a beginning more than an end. Decisions had to be made in the process of developing the model and in some cases there was not adequate information to permit unambiguous choices. As more experiments are carried out and, perhaps, more numerical calculations, some of the choices we have made may have to be modified. In any case, the model is simple enough to prove useful in analyzing future experiments. It is consistent internally and also with the experimental and theoretical data available thus far. Its success in predicting the properties of GeO_2 quantitatively and in describing more complicated solids than SiO_2 and GeO_2 [Paper II (Ref. 17)] is additional evidence that it is substantially correct.

*Work supported in part by the NSF Grant No. GH-39811.
†Portions of this work were carried out while at Stanford University, Stanford, California.

[1]H. R. Philipp, Solid State Commun. 4, 73 (1966).
[2]K. Platzöder, Phys. Status. Solidi. 29, K63 (1968).
[3]O. A. Ershov, D. A. Goganov, and A. P. Lukirskii, Fiz. Tverd. Tela 7, 2355 (1965) [Sov. Phys.-Solid State 7, 1903 (1966)].

[4]O. A. Ershov and A. P. Lukirskii, Fis. Tverd. Tela 8, 2137 (1966) [Sov. Phys.-Solid State 8, 1699 (1967)].
[5]T. H. DiStefano and D. E. Eastman, Solid State Commun. 9, 2259 (1971).
[6]G. Wiech, in *Soft-X-Ray Band Spectra*, edited by D. J. Fabian (Academic, New York, 1968).
[7]D. W. Fischer, J. Chem. Phys. 42, 3814 (1965); R. A. Mattson and R. C. Ehlert, Adv. X-Ray Anal. 9, 471 (1966); G. Klein and H.-U. Chun, Phys. Status Solidi B 49, 167 (1972).
[8]T. H. Di Stefano and D. E. Eastman, Phys. Rev. Lett. 27, 1560 (1971).
[9]H. Ibach and J. E. Rowe, Phys. Rev. B 10, 710 (1974).
[10]A. R. Ruffa, Phys. Status Solidi 29, 605 (1968); 25, 650 (1970).
[11]M. H. Reilly, J. Phys. Chem. Solids 31, 1041 (1970).
[12]A. J. Bennett and L. M. Roth, J. Phys. Chem. Solids 32, 1251 (1971); Phys. Rev. B 4, 2686 (1971).
[13]T. L. Gilbert, W. J. Stevens, H. Schrenk, M. Yoshimine, and P. S. Bagus, Phys. Rev. B 8, 5977.
[14]K. L. Yip and W. B. Fowler, Phys. Rev. B 10, 1400 (1974).
[15]A. R. Ruffa, J. Non.-Cryst. Solids 13, 37 (1973/74).
[16]There are two basic problems with such cluster calculations: (i) The convergence of the levels is rather poor as the size of the cluster is increased. Perhaps even larger clusters would improve the situation. (ii) Shapes of spectra cannot be reliably deduced from molecular orbital term values.
[17]S. T. Pantelides, Phys. Rev. B (to be published).
[18]W. A. Harrison, Phys. Rev. B 8, 4487 (1973).
[19]G. Lehman and J. Friedel, J. Appl. Phys. 33, 281 (1962).
[20]C. A. Coulson, L. R. Redei, and D. Stocker, Proc. R. Soc. Lond. 270, 357 (1962).
[21]W. A. Harrison and S. Ciraci, Phys. Rev. B 10, 1516 (1974).
[22]W. A. Harrison and J. Ch. Phillips, Phys. Rev. Lett. 33, 410 (1974).
[23]R. K. Sundfors, Phys. Rev. B 10, 4244 (1974).
[24]W. A. Harrison, Phys. Rev. 10, 767 (1974).
[25]D. J. Chadi, R. M. White, and W. A. Harrison, Phys. Rev. B (to be published).
[26]S. T. Pantelides and W. A. Harrison, Phys. Rev. B 11, 4049 (1975).
[27]S. T. Pantelides and W. A. Harrison, Phys. Rev. B 11, 3006 (1975).
[28]Extracted from R. W. G. Wyckoff, *Crystal Structures* (Interscience, New York, 1965), and the original references given therein.
[29]F. R. Boyd and J. L. England, J. Geophys. Res. 65, 749 (1960).
[30]See Ref. 21 for inclusion of S in this calculation.
[31]The definition of α_p is the same whether S is neglected or not.
[32]The use of the letter β instead of α is in anticipation of the fact that when we study $AlPO_4$ in paper II (Ref. 17) we will have to introduce still another polarity arising from the difference between Al and P, which is analogous to the polarity α_p of AlP. We will call this additional polarity *external polarity* and denote it by α_p. For obvious reasons we call β_p the *internal polarity*. Note that $\alpha_p = 0$ for SiO_2 as it is for Si.
[33]A prelimianry report of this has been made: S. T. Pantelides, Phys. Lett. A 54, 401 (1975). The parameters used there were slightly different.
[34]S. T. Pantelides, Phys. Rev. B 11, 5082 (1975); *ibid.* 13, 1843 (1976).
[35]L. P. Bouckaert, R. Smoluchowski, and E. Wigner, Phys. Rev. 50, 58 (1936).
[36]S. T. Pantelides (unpublished).
[37]J. D. Joannopoulos and M. L. Cohen, Phys. Rev. B 7, 2645 (1973).
[38]L. Ley, S. Kowalczyk, R. Pollak, and D. A. Shirley, Phys. Rev. Lett. 29, 1088 (1972).
[39]R. A. Pollack (private communication).
[40]Comparison with experiment is complicated by the fact that absolute values of intensities are hard to establish. Besides, different measurements of the same spectrum give different heights and even energy positions for the various features. See, e.g., Fig. 1 of Ref. 13.
[41]In Refs. 13 and 14 a Si_2O (Si-O-Si) cluster was employed in interpreting the O K emission spectrum. This is the smallest cluster with the correct topology for O excitations. In a recent paper, Tossell *et al.* [J. A. Tossell, D. J. Vaughan, and K. H. Johnson, Chem. Phys. Lett. 20, 329 (1973)] interpreted the O K spectrum in terms of the states of an SiO_4 cluster. The topology is then wrong and the interpretation is unreliable.
[42]See Ref. 6. The spectrum of Ref. 3 shows a small peak between the two main peaks which has led to speculation that d orbitals are present in the valence band states (Ref. 43); G. Wiech (private communication) has also seen this peak in some samples but has concluded that it is spurious and due to contaminants.
[43]G. A. D. Collins, D. W. J. Cruickshank, and A. Breeze, J. Chem. Soc. Faraday Trans. II 68, 1189 (1972).
[44]A. Koma and R. Ludeke, Phys. Rev. Lett. 35, 107 (1975).
[45]L. Pajasova, Czech. J. Phys. B 19, 1265 (1969).
[46]J. C. Phillips, Phys. Rev. B 9, 2775 (1974).
[47]S. T. Pantelides, Phys. Rev. B 11, 2391 (1975).
[48]S. T. Pantelides, D. J. Mickish, and A. B. Kunz, Phys. Rev. B 10, 2602 (1974).
[49]O. P. Rustgi and F. C. Brown, Phys. Rev. Lett. 28, 494 (1972).
[50]M. Altarelli and D. L. Dexter, Phys. Rev. Lett. 29, 1100 (1972).
[51]S. T. Pantelides, Solid State Commun. 16, 217 (1975).
[52]Based on a recalculation of the values listed in Ref. 21.
[53]See, e.g., J. M. Ziman, *Principles of the Theory of Solids* (Cambridge U. P., London, 1964), pp. 126 ff.
[54]See, e.g., C. Kittel, *Introduction to Solid State Phyics* (Wiley, New York, 1966), 3rd ed., p. 384; M. Born and K. Huang, *Dynamical Theory of Crystal Lattices* (Clarendon, Oxford, England, 1968), pp. 104 ff.; F. C. Brown, *The Phyics of Solids* (Benjamin, New York, 1967), p. 210.
[55]More complicated expressions, such as the Clausius-Mossotti form

$$(\epsilon-1)/(\epsilon+2)=\tfrac{4}{3}\pi(N_+\alpha_+ + N_-\alpha_-)$$

have also been used. This distinction does not have any bearing on the present discussion.
[56]S. T. Pantelides, Phys. Rev. Lett. 35, 250 (1975).
[57]The geometric factor g was not explicitly discussed in Ref. 56, particularly in conjunction with the compounds of the fluorite and antifluorite structure. See details in Ref. 58.
[58]S. T. Pantelides, Phys. Rev. B (to be published).

[59]J. M. Ziman, Ref. 48, p. 224.
[60]B. J. Skinner and D. E. Appleman, Am. Mineral. 48, 854 (1963)
[61]P. P. Keat, Science 120, 328 (1954).
[62]L. Coes, Jr., Science 118, 131 (1953).
[63]Landolt-Börnstein, *Zahlenwerte and Funktionen* (Springer, Berlin, 1962), Vol. 2, pt. 8.
[64]If the overlap S is included, more complicated expressions obtain.
[65]See, for example, F. C. Brown, Ref. 54, p. 93.
[66]F. C. Brown, Ref. 54, p. 101.
[67]Reference 66, p. 243.
[68]M. Blackman, Philos. Mag. 3, 831 (1959).
[69]R. M. Martin, Phys. Rev. B 1, 10 (1970).
[70]Reference 66, p. 97.
[71]C. Kittel, Ref. 54, p. 95.
[72]Reference 71, p. 84.
[73]D. A. Kleinman and W. G. Spitzer, Phys. Rev. 125, 16 (1963).
[74]R. E. Gibbs, Proc. R. Soc. Lond. 110, 443 (1926).
[75]S. Machlup and M. E. Christopher, J. Appl. Phys. 32, 1387 (1961).
[76]The only time the computer was used was in calculating the model densities of states of Figs. 3 and 4.